Geophys. J. R. astr. Soc. (1974) **36**, 411–459.

Earth Structure from Free Oscillations and Travel Times*

Thomas H. Jordan† and Don L. Anderson

(Received 1973 May 11)

Summary

An extensive set of reliable gross Earth data has been inverted to obtain a new estimate of the radial variations of seismic velocities and density in the Earth. The basic data set includes the observed mass and moment of inertia, the average periods of free oscillation (taken mainly from the Dziewonski–Gilbert study), and five new sets of differential travel-time data. The differential travel-time data consists of the times of $PcP-P$ and $ScS-S$, which contain information about mantle structure, and the times of $P'_{AB}-P'_{DF}$ and $P'_{BC}-P'_{DF}$, which are sensitive to core structure. A simple but realistic starting model was constructed using a number of physical assumptions, such as requiring the Adams–Williamson relation to hold in the lower mantle and core. The data were inverted using an iterative linear estimation algorithm. By using baseline-insensitive differential travel times and averaged eigenperiods, a considerable improvement in both the quality of the fit and the resolving power of the data set has been realized. The spheroidal and toroidal data are fit on the average to 0·04 and 0·08 per cent, respectively. The final model, designated model B1, also agrees with Rayleigh and Love wave phase and group velocity data.

The ray-theoretical travel times of P waves computed from model B1 are about 0·8 s later than the 1968 Seismological Tables with residuals decreasing with distance, in agreement with Cleary & Hales and other recent studies. The computed PcP, PKP, and $PKiKP$ times are generally within 0·5 s of the times obtained in recent studies. The travel times of S computed from B1 are 5–10 s later than the Jeffreys–Bullen Tables in the distance range 30° to 95°, with residuals increasing with distance. These S times are in general agreement with the more recent data of Kogan, Ibrahim & Nuttli, Lehmann, Cleary, and Bolt *et al.*

Model B1 is characterized by an upper mantle with a high, 4·8 km s^{-1}, S_n velocity and a normal, 3·33 g cm^{-3}, density. A low-velocity zone for S is required by the data, but a possible low-velocity zone for compressional waves cannot be resolved by the basic data set. The upper mantle transition zone contains two first-order discontinuities at depths of 420 km and 671 km. Between these discontinuities the shear velocity decreases with depth. The radius of the core, fixed by $PcP-P$ times and previous mode inversions, is 3485 km, and the radius of the inner core–outer core boundary is 1215 km. There are no other first-order discontinuities in the core model. The shear velocity in the inner core is about 3·5 km s^{-1}.

* Contribution No. 2279, Division of Geological and Planetary Sciences, California Institute of Technology, Pasadena, California.

† Present address: Department of Geological and Geophysical Sciences, Princeton University, Princeton, New Jersey.

1. Introduction

Prior to the last decade, estimates of the seismic velocities in the Earth were based almost exclusively on the information provided by travel-time observations. Since 1960, ultra-long period seismology has provided an important new source of data, the periods of the Earth's free oscillations. Besides sampling the velocity structure on a world-wide scale, eigenperiod data yields valuable constraints on the possible variations of density.

A number of recent studies have presented models of Earth's interior based on the inversion of free oscillation data (Gilbert & Backus 1968; Press 1968, 1970, 1972; Haddon & Bullen 1969; Derr 1969a; Dziewonski & Gilbert 1972; Wang 1972). These models yield significantly better fits to the mode data than models based on travel times alone. However, no model has been presented that satisfies both the eigenperiod and travel-time data to the precision that they are now known.

The purpose of this paper is to display a simple model of the average radial distributions of seismic velocities and density in the Earth derived from the inversion of the Earth's mass, moment of inertia, body-wave travel times, and periods of free oscillation. Using this model we investigate the consistency of seismological data that pertain to the spherically averaged Earth.

2. Approach

Deducing the constraints provided by observables on the variations of physical parameters in the Earth is an inverse problem. The mathematical formulation of this problem characterizes possible variations as entities in an abstract function space, each entity representing an Earth model. We shall assume that the Earth behaves as a spherically symmetric, non-rotating, elastic, and isotropic body to small mechanical excitations in the seismic frequency band (10^{-4} Hz$-$10 Hz), so that an Earth model is simply a radial variation of compressional velocity, shear velocity, and density. It is then a straightforward task to calculate from such a model its mass, moment of inertia, eigenperiods, and ray-theoretical travel times and compare them with observed data.

Of course, any particular observation of an eigenperiod or travel time will reflect the fact that the Earth is not spherically symmetric. Nevertheless, certain averages of eigenperiod and travel-time data will correspond to the data functionals of a well-defined spherically symmetric representation, called the Terrestrial Monopole by Gilbert (1971). This representation is the average of the distributions in the Earth over spheres concentric with its centre of mass. Using the zero-sum rule of first-order degenerate pertubation theory, Gilbert (1971) has shown that averages of eigenperiod data are unbiased estimators of the eigenperiods of the Terrestrial Monopole provided that, for each observation, the probability of picking a particular period as the peak period of a mode multiplet has a density equal to the density of singlets at that period. A similar result holds for travel times (Jordan 1972): To first order in the aspherical variations of velocity, the travel times between source-receiver pairs at constant angular distance are distributed with a mean equal to the travel time at that distance through the Terrestrial Monopole, provided that the distributions of sources and receivers on the surface of the Earth are uniform. These averaging rules motivate us to use averaged sets of free oscillation and travel-time data, and the Terrestrial Monopole is the representation we seek. Because no equivalent averaging rules exist at this time for amplitude, $dT/d\Delta$, and group velocity data, simple averages of these data do not necessarily correspond to data functionals of the Terrestrial Monopole. For this reason we have excluded these observations from the basic data set used in the inversion and have used them only to check the final model.

Unfortunately, with the present-day distribution of seismic sources and receivers

it is difficult to sample uniformly the velocity structure of the Earth's upper layers using body waves. In particular, the upper mantle under ocean basins is poorly sampled. Therefore, averaged sets of absolute travel-time data are generally biased. At teleseismic distances this bias enters into the distance-time relation approximately as a constant term or 'baseline error'. To reduce as much as possible the baseline error without eliminating the valuable information contained in travel-time data, we have used differential travel times; that is, the differences between the arrival times of two-body phases. If the phase combinations measured are judiciously chosen, their differential times will be relatively unbiased (Jordan 1972).

Because the distribution of physical parameters is continuous on some interval and the number of data is necessarily finite, the inverse problem generally has no unique solution. Furthermore, the observations used as data are invariably contaminated by errors; only estimates of the values of the data functionals for the Earth are available. Inaccuracies act to increase the ensemble of acceptable models.

A variety of techniques, both theoretical and computional, have been applied towards the solution of the geophysical inverse problem. One potentially powerful technique is the Monte Carlo method, described in the geophysical context by Keilis-Borok & Yanovskaya (1967) and applied to the determination of spherically symmetric Earth models by Press (1968, 1970, 1972). In practice, however, Monte Carlo techniques face severe limitations. Even with the most advanced computing systems the calculations are laborious and time consuming; the number of trials necessary to sample even very restricted regions of the model space is large. The more efficient algorithms such as the one used by Press (1972) require a sieve-like series of tests against the data: at each of several steps models are rejected or retained depending on how well they satisfy some subset of the data. Furthermore, in the Monte Carlo algorithm used by Press, *a priori* bounds are placed on the physical properties. Because the algorithm is intricate and the parameterization is severe, it is not clear in what way this procedure samples the ensemble of possible models. The principal advantage of the Monte Carlo method is that non-linear data functionals can be used directly without resorting to linear estimation. However, for calculations that use mode data, complete recomputation of the eigenperiods for each generated model is economically unfeasible. Instead, first-order variational parameters (Anderson 1964; Wiggins 1968; Anderson & Kovach 1969) have been used in published Monte Carlo studies (Press 1972), eliminating the principal advantage of the Monte Carlo technique.

At the present time the linear estimation method offers the most efficient and informative approach to the solution of geophysical inverse problem. Basically this method employs an iterative perturbation algorithm that approximates the differences between the sought representation of the Earth and some initial model as a particular solution to the finite system of linear, inhomogeneous integral equations that relate changes in the model to first-order changes in the data. The data functionals are computed for the initial model and subtracted from the observed data; the system of the perturbation equations is solved, and the calculated perturbation is added to the initial model. This sequence is iterated until an adequate fit is obtained.

The first-order approximation reduces the non-linear problem to solving an underdetermined system of linear equations. A general and extensive theory for the solution of the underconstrained linear inverse problem for inaccurately known data has been developed by Backus & Gilbert (1970). The central concept in this theory is the following: although the exact solution cannot be computed because the information provided by the data is insufficient, it is possible to estimate accurately *linear averages* of the desired model. They show that there exists a tradeoff between the ability to resolve detail and the accuracy with which this detail can be estimated.

We have used a variation of the Backus–Gilbert theory developed by Jordan & Franklin (1971), Jordan & Minster (1972), and Jordan (1972). A particular solution

to the linear system is obtained by minimizing a specified quadratic measure of error. This quadradic form is the sum of two terms, a measure of the resolution of the estimate and a measure of its accuracy, parameterized to yield a Backus–Gilbert type trade-off curve. Any particular solution computed by selecting a point on this trade-off curve can be shown to be an estimate of the sought solution convolved with a projection-like smoothing operator, termed the response operator of the system. Convolving the response operator with delta functions yields the averaging kernels.

The important aspect of this approach is that the model space is generalized to a Hilbert space with a fairly arbitrary norm, or measure of length. For this application we have chosen the norm to be a 'roughing' operator; that is, the inverse of a smoothing operator. The solution we shall use is the 'shortest' solution measured in this norm sense which will satisfy the data. Choosing the norm as a roughing operator means that, in measuring the solution's length, the high wave-number or 'rough' components are weighted more than low wave-number or 'smooth' components. Therefore, the high wave-number components are preferentially deleted. By this weighting scheme we can insure that the solution is smooth. We can allow for any number of discontinuities in the solution by choosing a discontinuous roughing operator. In fact, by manipulating this operator we can control to some degree the shape of the averaging kernels. Also, the use of this type of norm insures that the Fréchet kernels for travel times, which are not square-integrable, will have finite length.

3. The starting model

Because of the non-linear nature of the inverse problem, the success of an algorithm based on linear estimation depends critically on the model used to start the computation. In designing a starting model we must strike a balance between two opposing considerations. On the one hand, since eigenperiods and travel times are non-linear functionals, the starting model should be as linearly close as possible to the sought representation of the Earth. Otherwise, the model that results from successive perturbations may end up in a local minimum far removed from this representation, and the resolving power computations may be deceptive. Generally speaking, the starting model should include any major discontinuities that exist in the Earth. A starting model in which the velocities and density are taken to be constants is an example of an inadequate representation. On the other hand, we desire that the starting model be as 'simple' as possible—devoid of any features that might not exist in the spherically averaged Earth. For this reason published models generally make poor starting models.

The procedure we have adopted is to construct a starting model based on several simple physical assumptions. Central to these is the assumption that discontinuities in density and shear velocity are associated with discontinuities in compressional velocity. The corallary to this assumption has also been adopted: density and shear velocity will vary smoothly where the compressional velocity varies smoothly. The velocity profiles were constructed by requiring the model to fit certain observations of body wave travel times at teleseismic distances. Once the velocities were chosen, a density profile was obtained by the same procedure Birch (1964) used to construct his Model II.

The construction of the starting velocity model will be discussed region by region:

The crust (Bullen's region A)

The crust was modelled as a layer 21 km thick with $v_p = 6{\cdot}2\,\mathrm{km\,s^{-1}}$ and $v_s = 3{\cdot}4\,\mathrm{km\,s^{-1}}$. This roughly corresponds to an areal average of the six crustal types listed by Brune (1969): oceanic, shield, ridge, alpine, basin and range, and island arc.

The upper mantle and transition zone (regions B and C)

The presence of large radial velocity gradients and strong lateral variations complicates the interpretation of seismic data relevant to these regions of the mantle. Evidence from surface waves has confirmed Gutenberg's (1959) hypothesis that a low-velocity channel exists for shear waves in the upper 100 km or so of the mantle (Dorman, Ewing & Oliver 1960; Anderson 1967b). The structure of the transition region between 400 and 700 km has been illuminated by surface wave studies (Anderson & Toksöz 1963), $dT/d\Delta$ studies using large seismic arrays (Niazi & Anderson 1965; Johnson 1967), travel times from explosions (Ibrahim & Nuttli 1967; Kanamori 1967; Green & Hales 1968; Lewis & Meyer 1968; Nuttli 1969; Archambeau, Flinn & Lambert 1969; Julian & Anderson 1968), detailed studies of waveforms (Helmberger & Wiggins 1971), and precursors to the phase $P'P'$ (Adams 1971; Whitcomb & Anderson 1970). These studies have confirmed the presence of the two major discontinuities at depths near 400 and 650 km of Anderson & Toksöz (1963). However, the lateral variation of the upper mantle is great, as evidenced by the strong path dependence of body waves and surface waves, and the currently available data sample only a small fraction of the Earth's surface.

Because the average structure of these regions is in doubt, we have used a simple representation in the starting model. The compressional velocity below the crust was taken to be 8·0 km s^{-1}, linearly increasing to a value of 8·8 km s^{-1} at 420 km. The shear velocity in the upper mantle was taken to be a constant 4·55 km s^{-1}. Thus the starting model has no low-velocity zones in the upper mantle. Since the averaging kernels are quite localized in this region (see Section 6), the inversion method will generate a low velocity zone only if it is required by the data.

The transition region was modelled by two first-order discontinuities located at depths of 420 km and 671 km with the velocities varying linearly in between. At 420 km the compressional velocity jumps from 8·80 to 9·5 km s^{-1}, and the shear velocity jumps from 4·55 to 5·33 km s^{-1}. Between this depth and the discontinuity at 671 km, the compressional velocity increases at a rate of 0·27 km s^{-1} per 100 km, and the shear velocity is constant. These values were chosen on the basis of recent upper mantle models and were adjusted to agree with the teleseismic P times of the 1968 Tables (Herrin *et al.* 1968) and the teleseismic S times of Hales & Roberts (1970a).

The lower mantle (region D)

The velocities in the lower mantle increase uniformly with depth, similarly to the expected behaviour of a homogeneous material under adiabatic compression. Lower mantle models based on travel-time studies have changed very little since the early work of Gutenberg and Jeffreys. The travel times at large distances show little azimuthal dependence (Jeffreys 1962), and it has been inferred that the lateral heterogeneity of this region is small, at least in comparison with the upper mantle. Recent studies using more refined data indicate, however, that the lower mantle may be laterally variable (Alexander & Phinney 1966; Chinnery 1969; Davies & Sheppard 1972; Kanesewich *et al.* 1972; Julian & Sengupta 1973; Jordan 1972).

The initial compressional velocities in the lower mantle were taken from Herrin *et al.* (1968), and throughout most of the lower mantle the shear velocities of Randall (1971) were used. These studies used the same set of sources and involved relocation of the epicentres. In the lowermost mantle (region D''), Randall (1971) assumed a critical gradient for shear velocity. This feature was deleted by continuing his velocities smoothly to the core–mantle boundary. Both the compressional and shear velocity profiles taken from these studies were slightly smoothed.

The radius of the core

Since the radius of this discontinuity was fixed during the inversion, its accurate location for the starting model was critical. During the early inversion runs (Jordan, Minster & Anderson 1971) it became clear that modes sensitive to the radius of the core could not be satisfied with a core radius close to that of the Jeffreys–Bullen model or that used in the 1968 Tables (Taggart & Engdahl 1968). This suspicion was verified by a detailed study of $PcP-P$ differential travel times using both shallow and deep-focus events (Jordan & Anderson 1972). Assuming the lower mantle model of Herrin *et al.* (1968), we minimized the difference between the observed and computed times by varying the core radius, obtaining a final value of 3485 km. Since only differential times were used, our determination is insensitive to the upper mantle model assumed (the velocities we used were those described in the previous sub-sections). The radius obtained by this procedure is 12 km greater than the value obtained by Jeffreys, 8 km greater than Taggart's & Engdahl's (1968) value, and 10 km greater than the determination of Bolt (1968).

The suggestion that the core radius needs revision is not new. On the basis of readings of P and PcP, Kogan (1960) obtained a radius of 3486 km. In their early free oscillation work Bullen & Haddon (1967) suggested a value of 3493 km. From $ScS-S$ times Hales & Roberts (1971) made two estimates: $3489{\cdot}9\pm4{\cdot}7$ km and $3486{\cdot}1\pm4{\cdot}6$ km. Lehmann (1964) found that S was about 3·5 s late relative to the J–B Tables but that ScS agreed with the theoretical times. This would place the core–mantle boundary 13 km greater than the J–B value or at 3486 km.

The core (regions E, F and G)

A simple starting model for compressional velocity in the core was designed which fit most of the well-observed features of the PKP travel-time curve. It consists of an inner core and an outer core separated by a discontinuity located at 1215-km radius. The velocity at the core–mantle boundary was taken to be the same as Jeffreys' value ($8{\cdot}10$ km s^{-1}). The velocities in the outer core increase smoothly from this value to $10{\cdot}12$ km s^{-1} at the inner core–outer core boundary. A constant velocity of $11{\cdot}20$ km s^{-1} was adopted for the inner core.

In the starting model the transition region between the inner and outer cores is a simple discontinuity (the Lehmann discontinuity). The body wave evidence in support of a more complex transition region characterized by two or more discontinuities consists primarily of the high-frequency precursors to the P'_{DF} phase observed between 125° to 143° (Bolt 1962; Adams & Randall 1964). Interpretation of these arrivals has been a concern of seismologists since Gutenberg's early observational work. Gutenberg himself realized that these arrivals could not be interpreted in terms of a simple radial variation in velocity; he proposed instead a transition region in which the velocity varied with both radius and frequency. This interpretation was based on his observation that the precursors seem to be anomalously depleted in low frequencies, an observation that has been verified by Müeller (1973). To explain the anomalous frequency content of the precursor arrivals, their erratic behaviour, and the large curvature attributed to this ' branch ' of the travel-time curve (Buchbinder 1971), Haddon (1972) has recently proposed that they are the result of scattering off heterogeneities located somewhere in the vicinity of the mantle–core interface. Although to explain these arrivals by heterogeneity in this region would require large amplitude variations (for example, bumps on the core–mantle boundary with amplitudes greater than 10 km (Jordan 1972)), scattering off some sort of velocity heterogeneity (perhaps, in the vicinity of the inner core–outer core transition) is the most satisfactory explanation.

The compressional velocity starting model fits the times of the AB and DF branches in the 1968 Tables (Bolt 1968) to within 2 s.

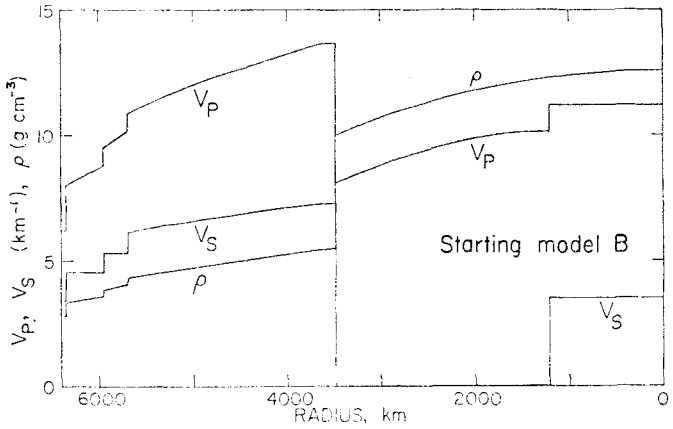

FIG. 1. Starting model B.

In our starting model the inner core was assumed to be solid with a shear velocity of 3·5 km s^{-1}. Birch (1940) first suggested that the Lehmann discontinuity indicated a liquid–solid transition in his paper on the phase relations in iron. Bullen (1946, 1958) based his arguments for solidity of the inner core on his hypothesis that the compressibility of the material in the deep interior is nearly continuous as a function of depth. Early free oscillation work supported this concept (Alsop 1963; Anderson & Smith 1968; Derr 1969a); introducing a solid inner core allowed a better fit to the radial modes. However, the first precise determination of the shear velocity in the inner core was made by Dziewonski & Gilbert (1972) from more complete observations of modes sensitive to this parameter (the radial modes ${}_0S_0 - {}_4S_0$ and the spheroidal overtones ${}_2S_2$, ${}_5S_2$, ${}_8S_2$). We have adopted their value of 3·5 km s^{-1}.

The initial density model

Once the velocity distributions had been constructed, we determined the density distribution from the values of the Earth's mass and moment of inertia using a procedure due to Birch (1964). The density of the crust was assumed to be 2·79 g cm^{-3}. In the upper mantle and transition region we required the density to satisfy Birch's relation: $\rho = av_p + b$, where a and b are constants. The density at the top of the mantle was taken to equal 3·33 g cm^{-3} yielding the value 0·54 g cm^{-3} for b. Below the discontinuity at 671 km, the density was determined by integrating the Adams–Williamson equations for a homogeneous substance in adiabatic compression (Bullen 1963, p. 229). At the top of the core the Adams–Williamson equations were re-initiated with a new value of the density, ρ_c, and the integration was continued to the centre. The density was taken to be continuous across the Lehmann discontinuity. The two free parameters a and ρ_c were determined by fitting the mass and moment of inertia. The values obtained were 0·349 and 9·98, respectively, which can be compared with Birch's values of 0·379 and 9·96 for his solution II.

The starting model is shown in Fig. 1.

4. The basic data set

The basic data set consisted of 219 data. Of these, 178 were normal mode periods, 39 were differential travel times, and the remaining two were the Earth's mass M and moment of inertia I.

Normal mode data

Gilbert (1971) observed that the average period of singlets in a mode multiplet split by disturbing influences such as rotation, ellipticity of figure, and the presence of lateral heterogeneities equals, to a first-order approximation, the degenerate eigenperiod of a spherically averaged Earth model. Unfortunately, resolution of the multiplet structures of eigenperiods is, with the exception of only the gravest modes, impossible at the present time. Instead we must rely on averages of many observations to give periods that can be interpreted in terms of an average Earth structure.

Averages of the observed free oscillation periods were given by Pekeris in 1966. However, the wide variations in the quality of the early recordings, mainly from the Chilean earthquake of 1960, and the procedures used to reduce the data largely negated the advantage of using these averages; much of the early inversion work was done with values obtained from individual records. Anderson (1967b) also presented averages but selected 'best values' based on record and spectrum quality to evaluate various Earth models. As investigators have set themselves to the task of gleaning from the existing records information about the mode spectrum, the situation has improved considerably. Derr (1969b) averaged the observations available through 1968 using a complex, somewhat arbitrary system of weights to enhance the importance of the higher resolution recordings. Although the great majority of the more than 1500 data he used were of the fundamental mode, he attempted to obtain averages of some of the higher modes as well. Unfortunately, some of his mode designations (e.g. ${}_1S_0$, ${}_1S_6$, ${}_1S_7$) are in error.

Backus & Gilbert (1968) have shown that inclusion of higher modes dramatically improves the resolving power of the normal mode data set. Recently, a major contribution to the study of the normal mode spectrum has been made by Dziewonski & Gilbert (1972). Using a comprehensive series of criteria to identify modes, they have analysed 84 long-period seismograms of the great Alaskan earthquake of 1964 and tentatively identified all but 30 of the 136 theoretically predicted multiplets in the normal mode spectrum with periods greater than 300 s, as well as a number of modes in the period range 200–300 s. Besides their extensive listing of higher-mode periods, they also gave averages of the available fundamental mode data for periods greater than 176 s (${}_0S_3 - {}_0S_{50}$, ${}_0T_3 - {}_0T_{46}$). Their averages, listed with standard errors in the means in Tables 2–5 of their paper, formed the basis of our normal mode data set. They were unable to detect the lowest order modes (${}_0S_2$ and ${}_0T_2$) and therefore did not list averages. For these modes and for ${}_0S_3$ we have used the periods given by Derr (1969b). In addition, we included in our data set the average periods of the modes ${}_0S_{51} - {}_0S_{63}$ given in Table 3 of Dziewonski (1971). These data are listed with the eigenperiods of our final model in Tables A1 and A2. The remarkable consistency of this data set is indicated by the precision with which the final model fits the data.

Average value for the shorter period fundamental mode free oscillation data have also been obtained from the great-circle dispersion studies of Toksöz & Ben-Menahem (1963), Kanamori (1970), Dziewonski & Landisman (1970), and Dziewonski, Mills & Bloch (1972). We will compare the dispersion curves calculated from our final model with these studies in Section 7.

The travel-time data set

Because of the problem with baseline bias in absolute travel times, we have used only differential travel times in the inversion. By using differential travel times the effects of inhomogeneities in the upper mantle and uncertainties due to source mislocation are virtually eliminated (Jordan 1972).

Surface focus $PcP - P$ times were reduced from the published absolute travel times of PcP and P recorded from nuclear explosions and reported by Kogan (1960),

Buchbinder (1965), Kanamori (1968), and Lambert *et al.* (1968). Differential travel times of core phases $P'_{AB}-P'_{DF}$ and $P'_{BC}-P'_{DF}$ were obtained from the raw data of Hai (1963) and Engdahl (1968) and supplemented by new readings from three deep-focus events in the Sunda Arc. All of the above readings were measured from short-period vertical seismograms. Two new sets of differential travel times for the phase combinations $PcP-P$ and $ScS-S$ were generated for this study (Jordan 1972) from long-period WWSSN records using eleven deep-focus earthquakes. A particular effort was made to obtain a global distribution of sources and receivers.

The 5° cell means (computed as J–B residuals) and standard errors in the means for the differential travel-time data are listed in Table A3. The raw times and a more complete discussion of the observations are given by Jordan (1972). Comparison of the mean $PcP-P$ travel times for the two depths of focus shows that they are mutually consistant at the 90 per cent confidence level. Surprisingly, these results differ at this same significance level from the 1968 Tables. Although the 1968 Tables show the same general trend, they are up to one second later than the observed times at distances in the range 30°–50°. The $P'_{AB}-P'_{DF}$ times are generally consistant with the 1968 Tables, but the $P'_{BC}-P'_{DF}$ times are not. The $ScS-S$ times average about one second greater than the J–B Tables, although the residuals are somewhat larger at distances less than 40°. Considering that nearly 200 high-quality $ScS-S$ readings were used in this study, standard errors in the cell means are quite large. This reflects the fact that the $ScS-S$ times show a large scatter (up to 10 s) most probably due to lateral heterogeneity in the lower mantle (Hales & Roberts 1970b; Jordan 1972).

Inclusion of the differential travel times increases considerably the resolving power of our data set. This resolving power cannot be obtained from the presently observed eigenperiods alone (Jordan & Anderson 1972). The increase in resolving power is most dramatic in the lower mantle and near the inner core–outer core boundary.

Sets of differential travel times exist for the phase combinations $SKS-S$ (Hales & Roberts 1970a) and SKKS–SKS (Hales & Roberts 1971). Although we have not used these data in the inversion, they provide a check on the inversion results (see Table A4).

Mass and moment of inertia

We used the values of the mass M and normalized moment of inertia I/MR^2 given by Jeffreys (1970). These are

$$M = 5{\cdot}977 \pm 0{\cdot}0006 \times 10^{27}$$

$$I/MR^2 = 0{\cdot}330841 \pm 0{\cdot}00018.$$

5. The inversion algorithm

An estimate of the difference $\delta\mathbf{m}$ between the actual representation $\mathbf{m}_0$ of the spherically averaged Earth and some initial guess $\mathbf{m}_s$ can be approximated as a solution of the linear equation

$$A\delta\mathbf{m}+\mathbf{n} = \delta\mathbf{d}, \tag{1}$$

where $\delta\mathbf{d}$ is a vector whose components are the differences between the observed and the computed values of the data, A is the linear operator whose row elements are the Fréchet kernels of the data, and $\mathbf{n}$ is a vector of errors associated with the data. If the noise process is assumed to be a Gaussian process with zero mean and autocorrelation operator C_{nn}, then the best estimate of the solution is given by (Jordan & Minster (1972), Jordan (1972))

$$\delta\mathbf{m} = C_{ss}A^T(AC_{ss}A^T+\tan\theta\, C_{nn})^{-1}\delta\mathbf{d}, \tag{2}$$

where A^T is the transpose of A, C_{ss} is the solution autocorrelation operator whose inverse defines the norm on the space of Earth models, and θ is the parameter of the trade-off curve ($0 < \theta < \pi/2$). The averaging kernels associated with this estimate are the row elements of the operator

$$\mathscr{A} = C_{ss} A^T (A C_{ss} A^T + \tan\theta C_{nn})^{-1} A. \tag{3}$$

Equation (2) yields the 'smallest' estimate of the true solution, in a norm sense, that is consistent with the data; i.e. the quadratic form $\delta\mathbf{m} C_{ss}^{-1} \delta\mathbf{m}$ is minimized subject to the constraint equation (1). To insure that the solution behaves smoothly between discontinuities, we choose C_{ss} to be a block-diagonal operator with blocks bounded by the first-order discontinuities in the starting model. Each of the blocks is taken to be a smoothing operator parameterized by a correlation wavelength λ. The specific form we use has been derived by Jordan (1972, eqn. 5.2.6) following a procedure outlined by Jordan & Minster (1972). For this particular form, assigning a correlation wavelength λ implies that the components of $\delta\mathbf{m}$ of wavelength λ are weighted twice as much as the infinite wavelength or constant components in the minimization. Thus, 'smooth' solutions will be shorter (i.e. smaller) than 'rough' solutions when measured by this norm.

To specify the matrix C_{nn} we assume that the errors in the data are uncorrelated. Then C_{nn} is a diagonal matrix whose ith diagonal element is the variance of the ith datum.

Because the computer available to us was fairly small (an IBM 370/155 with 80K words of core), it was not feasible to invert all three functions v_p, v_s, and ρ simultaneously. Instead, a FORTRAN program was written capable of inverting either the compressional velocity and the density or the shear velocity and the density simultaneously. An iteration scheme employing the estimate given by equation (2) was designed which alternate between these two possibilities. At each step up to eighty data could be inverted. Convergence was rapid as long as $\tan\theta$ was kept at a value greater than five. Typically, a run involving one iteration on a data set consisting of 50 normal modes and 30 travel times required about 20 min and cost about $50.00.

6. Inversion results—model B1

Using the inversion algorithm described in the previous section, the data set presented in Section 4, and the starting model constructed in Section 3, we have derived an estimate of the radial velocity and density distributions. The model obtained has been designated model B1.

The starting model, model B, fit the eigenperiods of the basic data set with a root mean square (RMS) relative deviation of about 0·3 per cent, and the computed differential travel times deviated from the observed by at most 3 s (for $ScS-S$ at 30°). Thus, considering the simplicity of the starting model, it is a good fit to the data. (Press (1972) in his Monte Carlo work, for example, accepted models which fit most of the observed periods within 0·4 per cent.) Such a fit indicates that the starting model is not far removed from the spherically averaged representation of the Earth which, as we emphasized in Section 3, is usually necessary to insure the success of a linear estimation algorithm.

The correlation operator C_{ss} appearing in equation (2) was chosen so that the perturbations to the three functions v_p, v_s, and ρ were independent; i.e. the elements of C_{ss} corresponding to the cross-correlation between any two of these functions were taken to be zero. Also, the model functions were uncorrelated between regions separated by first-order discontinuities in the starting model. For example, the perturbations to density in the lower mantle were uncorrelated with perturbations to density in the outer core. This allowed first-order discontinuities in the velocity and density perturbations at the radii of the discontinuities in the starting model

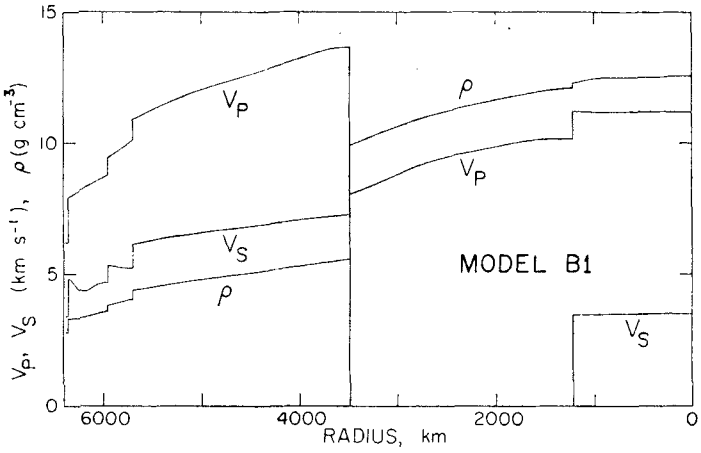

FIG. 2. Model B1.

(1215 km, 3485 km, 5700 km, 5951 km and 6350 km). The correlation wavelengths of each of the model functions were chosen to be 1000 km in the inner core, the outer core (except for v_s which was not inverted in this region), and the lower mantle. Two hundred kilometre wavelengths were assigned to the density perturbation in the transition region (5700–5951 km), and 100-km wavelengths were assigned to the velocity functions. In the upper mantle the correlation wavelengths for the velocities were chosen to be 100 km, and the correlation wavelength for the density was chosen to be 300 km. The velocities and density of the crust were not inverted.

Convergence to the final model was achieved in eight iterations. This model, B1, is shown in Fig. 2 and listed in Table 1. Besides the model functions v_p, v_s, and ρ, we have also listed the values of the seismic parameter $\Phi = v_p^2 - (4/3)v_s^2$, the bulk modulus K, the shear modulus μ, the Lamé parameter λ, Poisson's ratio σ, the pressure, and the gravitational acceleration. The values of the data functionals for B1 are compared with the observations in the Appendix. The fit of these data will be discussed in Sections 7 and 8.

Fig. 3 shows the total perturbation (B1–B) for this inversion. It can be seen from this figure that the differences between B1 and the starting model are quite small.

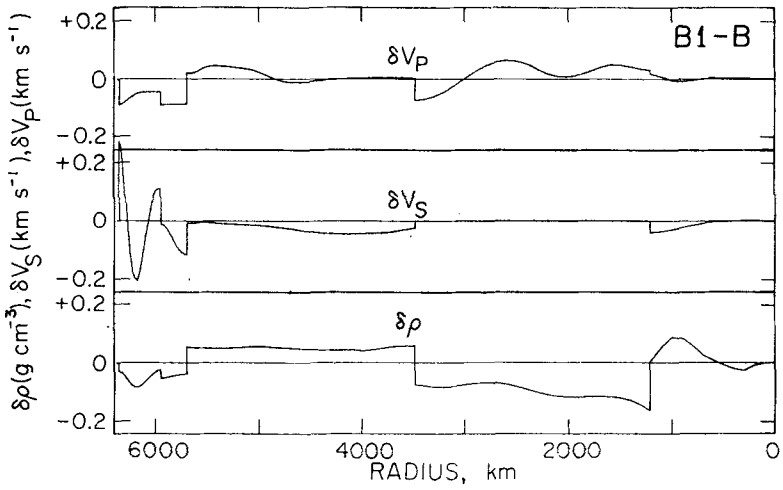

FIG. 3. The total perturbation; i.e. the difference between model B and B1.

Table 1

*Model B*1

Index	Radius (km)	Depth (km)	v_p (km s^{-1})	v_s (km s^{-1})	ρ (g cm^{-3})	Φ (km^2 s^{-2})	K (Kb)	μ (Kb)	λ (Kb)	σ	Pressure (Kb)	g (cm s^{-2})
1	1	6370	11.20	3.50	12.58	109.11	13721	1540	12694	0.4459	3609	0
2	100	6271	11.20	3.50	12.57	109.11	13716	1541	12689	0.4459	3606	52
3	200	6171	11.20	3.50	12.56	109.12	13700	1539	12674	0.4458	3598	78
4	300	6071	11.20	3.50	12.53	109.14	13671	1535	12648	0.4459	3586	110
5	400	5971	11.20	3.50	12.52	109.16	13665	1532	12643	0.4459	3570	144
6	500	5871	11.20	3.50	12.51	109.18	13663	1531	12642	0.4460	3550	178
7	600	5771	11.20	3.50	12.51	109.20	13658	1528	12639	0.4461	3525	212
8	700	5671	11.20	3.49	12.50	109.19	13649	1523	12633	0.4462	3496	247
9	800	5571	11.19	3.48	12.50	109.12	13644	1517	12632	0.4464	3463	281
10	900	5471	11.19	3.48	12.49	109.09	13630	1510	12623	0.4466	3426	316
11	1000	5371	11.19	3.47	12.46	109.22	13609	1499	12610	0.4469	3384	350
12	1100	5271	11.21	3.46	12.39	109.57	13571	1485	12581	0.4472	3339	385
13	1215	5156	11.22	3.46	12.28	109.87	13492	1467	12513	0.4475	3281	423
14	1215	5156	10.14	0.0	12.11	102.91	12460	0	12460	0.5000	3281	423
15	1300	5071	10.15	0.0	12.08	102.99	12444	0	12444	0.5000	3236	450
16	1400	4971	10.15	0.0	12.04	103.06	12411	0	12411	0.5000	3180	482
17	1500	4871	10.14	0.0	11.99	102.85	12334	0	12334	0.5000	3120	514
18	1600	4771	10.12	0.0	11.93	102.39	12219	0	12219	0.5000	3056	546
19	1700	4671	10.07	0.0	11.87	101.47	12042	0	12042	0.5000	2990	578
20	1800	4571	10.00	0.0	11.80	100.08	11805	0	11805	0.5000	2919	609
21	1900	4471	9.93	0.0	11.72	98.65	11561	0	11561	0.5000	2846	640
22	2000	4371	9.86	0.0	11.64	97.14	11307	0	11307	0.5000	2769	671
23	2100	4271	9.78	0.0	11.56	95.59	11048	0	11048	0.5000	2690	701
24	2200	4171	9.70	0.0	11.47	94.00	10785	0	10785	0.5000	2607	731
25	2300	4071	9.62	0.0	11.39	92.57	10542	0	10542	0.5000	2522	760
26	2400	3971	9.55	0.0	11.30	91.23	10309	0	10309	0.5000	2434	790
27	2500	3871	9.46	0.0	11.21	89.51	10032	0	10032	0.5000	2343	818
28	2600	3771	9.35	0.0	11.11	87.49	9718	0	9718	0.5000	2250	846
29	2700	3671	9.24	0.0	11.00	85.35	9388	0	9388	0.5000	2155	874
30	2800	3571	9.11	0.0	10.88	82.92	9023	0	9023	0.5000	2058	901
31	2900	3471	8.96	0.0	10.76	80.21	8628	0	8628	0.5000	1959	928
32	3000	3371	8.79	0.0	10.62	77.30	8209	0	8209	0.5000	1858	954
33	3100	3271	8.63	0.0	10.48	74.41	7797	0	7797	0.5000	1756	979
34	3200	3171	8.46	0.0	10.33	71.62	7400	0	7400	0.5000	1653	1003
35	3300	3071	8.31	0.0	10.19	68.99	7026	0	7026	0.5000	1549	1026
36	3400	2971	8.16	0.0	10.04	66.52	6676	0	6676	0.5000	1444	1049
37	3485	2886	8.02	0.0	9.90	64.36	6373	0	6373	0.5000	1354	1068
38	3485	2886	13.67	7.27	5.58	116.38	6489	2948	4523	0.3027	1354	1068
39	3510	2861	13.67	7.27	5.56	116.35	6466	2934	4510	0.3029	1340	1064
40	3550	2821	13.66	7.26	5.54	116.32	6443	2916	4498	0.3033	1316	1059

Table 1 (*continued*)

Index	Radius (km)	Depth (km)	v_p (km s^{-1})	v_s (km s^{-1})	ρ (g cm^{-3})	Φ (km^2 s^{-2})	K (Kb)	μ (Kb)	λ (Kb)	σ	Pressure (Kb)	g (cm s^{-2})
41	3625	2746	13.63	7.22	5.50	116.09	6385	2871	4471	0.3045	1272	1049
42	3700	2671	13.57	7.19	5.46	115.28	6294	2822	4412	0.3049	1229	1041
43	3775	2596	13.49	7.16	5.42	113.67	6160	2775	4309	0.3041	1187	1034
44	3850	2521	13.40	7.13	5.38	111.84	6014	2730	4194	0.3029	1145	1027
45	3925	2446	13.31	7.09	5.34	109.99	5870	2686	4079	0.3015	1104	1021
46	4000	2371	13.22	7.06	5.30	108.16	5727	2642	3966	0.3001	1063	1016
47	4075	2296	13.13	7.03	5.26	106.36	5597	2601	3863	0.2988	1023	1011
48	4150	2221	13.03	6.99	5.22	104.68	5469	2555	3765	0.2979	984	1008
49	4225	2146	12.95	6.96	5.19	103.12	5347	2509	3674	0.2971	944	1004
50	4300	2071	12.86	6.92	5.15	101.55	5227	2465	3583	0.2962	905	1001
51	4375	1996	12.77	6.88	5.11	99.84	5102	2422	3487	0.2951	867	999
52	4450	1921	12.68	6.85	5.07	98.13	4978	2380	3391	0.2938	829	997
53	4525	1846	12.59	6.81	5.04	96.63	4866	2336	3309	0.2931	791	996
54	4600	1771	12.50	6.77	5.00	95.13	4755	2293	3226	0.2923	754	994
55	4675	1696	12.41	6.74	4.96	93.49	4638	2253	3136	0.2909	716	994
56	4750	1621	12.33	6.71	4.92	92.10	4535	2214	3058	0.2901	680	993
57	4825	1546	12.25	6.67	4.89	90.62	4427	2174	2977	0.2890	643	993
58	4900	1471	12.16	6.64	4.85	88.99	4313	2136	2888	0.2874	607	993
59	4975	1396	12.06	6.59	4.81	87.59	4211	2089	2819	0.2872	571	993
60	5050	1321	11.97	6.55	4.77	86.07	4103	2044	2740	0.2864	535	993
61	5125	1246	11.86	6.50	4.72	84.34	3984	1998	2651	0.2851	500	994
62	5200	1171	11.75	6.47	4.68	82.36	3854	1956	2549	0.2829	465	994
63	5275	1096	11.64	6.44	4.64	80.15	3715	1920	2435	0.2796	430	995
64	5350	1021	11.52	6.39	4.59	78.30	3594	1871	2346	0.2781	395	996
65	5425	946	11.39	6.33	4.55	76.31	3469	1824	2253	0.2763	361	997
66	5500	871	11.26	6.28	4.50	74.19	3340	1778	2154	0.2739	327	998
67	5550	821	11.17	6.25	4.47	72.72	3252	1746	2087	0.2722	305	999
68	5600	771	11.07	6.21	4.44	71.18	3162	1712	2020	0.2706	283	1000
69	5650	721	10.97	6.17	4.41	69.71	3075	1677	1957	0.2693	261	1000
70	5700	671	10.88	6.12	4.38	68.39	2996	1642	1901	0.2683	239	1001
71	5700	671	10.08	5.21	4.05	65.37	2644	1098	1911	0.3175	239	1001
72	5725	646	10.01	5.21	4.02	64.03	2575	1092	1846	0.3141	228	1001
73	5750	621	9.95	5.22	4.00	62.62	2503	1088	1777	0.3100	218	1000
74	5775	596	9.88	5.23	3.97	61.16	2433	1086	1706	0.3055	208	1000
75	5800	571	9.81	5.24	3.95	59.66	2355	1084	1632	0.3004	199	1000
76	5825	546	9.75	5.26	3.92	58.13	2280	1084	1558	0.2948	189	999
77	5850	521	9.68	5.27	3.90	56.58	2205	1084	1482	0.2887	179	999
78	5875	496	9.61	5.29	3.87	55.05	2131	1084	1408	0.2825	169	999
79	5900	471	9.54	5.31	3.85	53.56	2060	1083	1338	0.2763	160	998
80	5925	446	9.48	5.32	3.82	52.14	1992	1079	1272	0.2705	150	998

Table 1 (*continued*)

Index	Radius (km)	Depth (km)	v_p (km s^{-1})	v_s (km s^{-1})	ρ (g cm^{-3})	Φ (km^2 s^{-2})	K (Kb)	μ (Kb)	λ (Kb)	σ	Pressure (Kb)	g (cm s^{-2})
81	5951	420	8.41	5.32	3.80	50.76	1926	1074	1210	0.2649	140	997
82	5951	420	8.75	4.67	3.58	47.61	1706	780	1186	0.3017	140	997
83	5975	396	8.71	4.66	3.57	46.79	1668	775	1151	0.2988	132	997
84	6000	371	8.66	4.66	3.54	46.02	1630	768	1118	0.2965	124	996
85	6050	321	8.56	4.60	3.49	44.96	1569	739	1076	0.2964	105	994
86	6100	271	8.46	4.50	3.44	44.53	1530	695	1067	0.3028	88	992
87	6150	221	8.35	4.37	3.39	44.26	1498	648	1066	0.3110	71	990
88	6175	196	8.30	4.34	3.37	43.79	1473	633	1051	0.3119	63	989
89	6200	171	8.25	4.35	3.35	42.77	1432	633	1009	0.3072	54	988
90	6225	146	8.19	4.37	3.34	41.60	1388	637	962	0.3008	46	987
91	6250	121	8.13	4.44	3.33	39.88	1327	656	889	0.2878	38	986
92	6271	100	8.08	4.53	3.32	38.05	1264	681	810	0.2717	31	986
93	6271	100	8.08	4.53	3.32	38.05	1264	681	810	0.2717	31	986
94	6290	81	8.04	4.62	3.32	36.21	1202	708	730	0.2537	25	985
95	6310	61	8.00	4.72	3.32	34.24	1135	738	643	0.2327	18	984
96	6330	41	7.95	4.80	3.31	32.52	1076	762	568	0.2136	12	984
97	6350	21	7.91	4.83	3.30	31.45	1037	769	524	0.2026	5	983
98	6350	21	6.20	3.40	2.79	23.03	642	322	427	0.2850	5	983
99	6360	11	6.20	3.40	2.79	23.03	642	322	427	0.2850	3	982
100	6371	0	6.20	3.40	2.79	23.03	642	322	427	0.2850	0	981

Table 2

Mode misfits (T > 300 *s*) *and possibly contaminating modes with periods greater than* 300 *s. A mode is listed as a misfit if its period computed for B*1 *lies outside the* 95 *per cent confidence interval for the datum.*

Mode	Obs. period (s)	95% C.I. (s)	B1 period (s)	B1–Obs. (s)	Possible contaminants mode	Period (s)
${}_0S_7$	811·45	0·50	812·24	+0·79		
${}_0S_{10}$	580·08	0·18	579·19	−0·89	${}_3S_2$	580·49
${}_0S_{11}$	536·56	0·22	536·87	+0·31	${}_2S_7$	535·77*
${}_0S_{14}$	448·28	0·10	448·10	−0·18	${}_2S_9$	448·37
${}_0S_{17}$	389·31	0·14	389·56	+0·25	${}_2S_{11}$	388·54
${}_0S_{18}$	373·89	0·14	374·10	+0·21	${}_3S_7$	372·45
${}_0S_{20}$	347·82	0·14	347·47	−0·35	${}_6S_1$	348·32
${}_1S_4$	852·68	0·74	851·75	−0·93		
${}_1S_5$	730·56	1·00	729·30	−1·26	${}_2S_4$	725·02
${}_1S_6$	657·61	0·41	656·94	−0·67	${}_2S_5$	660·44*
${}_1S_8$	555·83	0·16	556·22	+0·39		
${}_1S_{10}$	465·45	0·63	466·20	+0·75		
${}_1S_{14}$	337·00	0·16	336·64	−0·26	${}_0S_{21}$	335·88
${}_1S_{15}$	316·06	0·17	315·59	−0·47	${}_0S_{23}$	315·38
${}_2S_8$	488·02	0·33	487·65	−0·27	${}_3S_3$	488·00
${}_2S_{15}$	309·20	0·15	308·95	−0·25	${}_7S_2$	309·58
${}_3S_3$	489·05	0·82	488·00	−1·05	${}_2S_8$	487·65
${}_3S_7$	372·05	0·28	372·45	+0·40	${}_4S_5$	369·88
${}_3S_8$	354·57	0·23	354·86	+0·29	${}_5S_3$	354·22
${}_3S_{10}$	323·80	0·23	324·41	+0·61	${}_0S_{22}$	325·23
${}_4S_1$	505·82	0·45	504·14	−1·68		
${}_4S_2$	479·33	0·38	478·00	−1·33		
${}_5S_2$	397·36	0·36	396·78	−0·58	${}_2S_0$	398·49
${}_5S_3$	353·52	0·42	354·22	+0·70	${}_3S_8$	354·86
${}_7S_2$	310·07	0·17	309·58	−0·49	${}_3S_{11}$	310·68
${}_0T_7$	819·31	1·41	817·76	−1·55		
${}_0T_8$	736·86	0·68	736·13	−0·73		
${}_0T_{14}$	475·73	0·75	476·73	+1·00	${}_1T_7$	475·34*
${}_0T_{15}$	450·97	0·54	451·71	+0·74	${}_5S_1$	450·72*
					${}_2T_2$	449·22*
${}_0T_{17}$	407·95	0·42	409·35	+1·40	${}_1T_9$	408·17
					${}_0S_{16}$	406·76
${}_1T_{10}$	381·58	0·33	382·07	+0·49	${}_2T_6$	383·74*
${}_2T_4$	421·81	0·78	420·62	−1·19		

* Period computed for UTD 124A (Dziewonski & Gilbert 1972).

Except for shear velocity in the upper mantle, the total perturbation is nowhere greater than 0·2 units of velocity (km s^{-1}) or density (g cm^{-3}); and it is generally less than 0·1 units. Since B1 is an excellent fit to the data we used, the small magnitude of the perturbation further justifies the use of model B as a starting model. It also demonstrates the stability of the inversion algorithm.

A detailed discussion of the perturbation requires inspection of the averaging kernels; i.e. the rows of the operator $\mathscr{A}$ given by equation (3). The averaging kernels computed for B1 using the two data sets ($v_p-\rho$ and $v_s-\rho$) are shown for selected radii in Fig. 4. The operator $\mathscr{A}$ has the property that, if $\mathbf{m}_0$ is the spherically averaged Earth, if $\delta\mathbf{m}$ is the perturbation obtained in the inversion, and if the starting model $\mathbf{m}_s$ is in the linear neighbourhood of $\mathbf{m}_0$, then $\delta\mathbf{m}$ is an estimate of $\mathscr{A}(\mathbf{m}_0-\mathbf{m}_s)$. This just says that $\delta\mathbf{m}$ is a filtered version of the perturbation we seek, $\mathscr{A}$ being the filter. As we stated in the last section, $\delta\mathbf{m}$ is in some sense the smallest possible perturbation

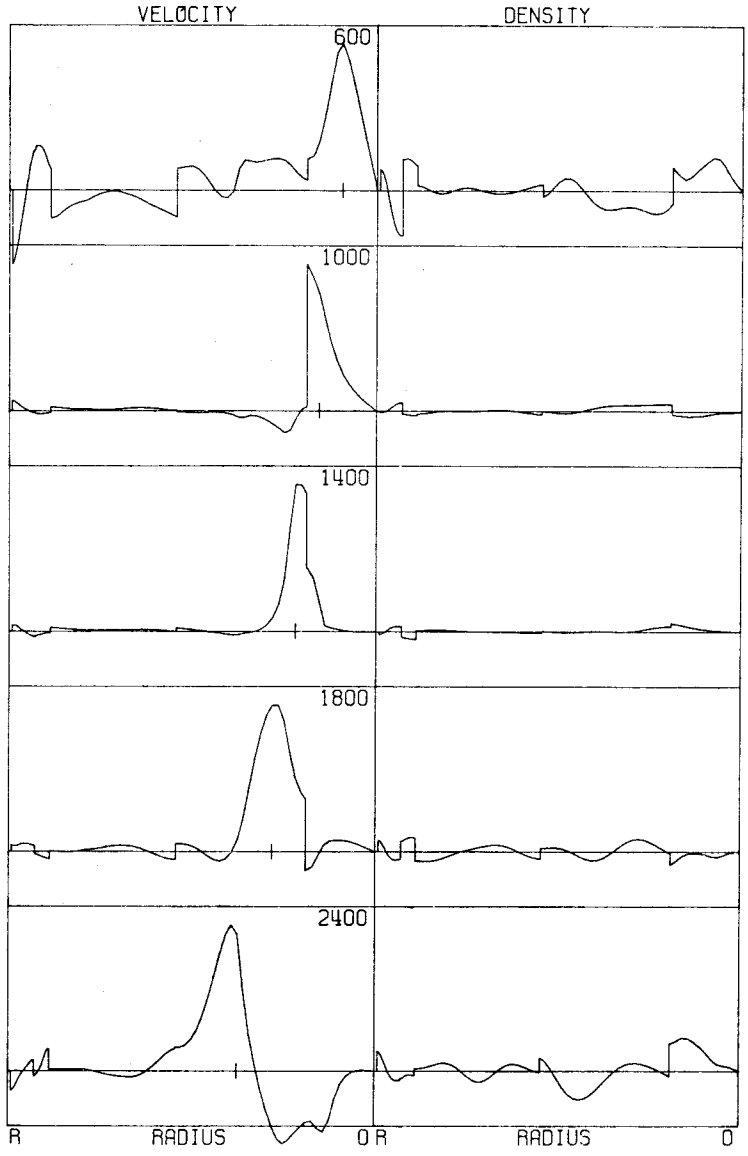

FIG. 4(a). See caption, p. 428.

that will yield a model consistent with the data. This does not imply, however, that every detail of this estimate is required by the data. Roughly speaking, for a feature located at radius r_0 in, say, the density solution to be required by the data, it is necessary that the row of $\mathscr{A}$ corresponding to the averaging of density at r_0 be localized about r_0 in a peak with width less than the predominant scale length of that feature (Backus & Gilbert 1970). Even this criterion is not sufficient to insure resolvability. We must also require that the perturbation be large enough in magnitude to significantly improve the fit to the data.

Inspection of the averaging kernels in Fig. 4 reveals that in regions of continuity the perturbation shown in Fig. 3 has no predominant scale lengths less than the peak widths of the averaging kernels. However, the averaging is not everywhere localized. In particular, the density kernels at radii less than 2400-km radius are poorly localized. By poorly localized we mean that they either have less than 50 per cent of their area

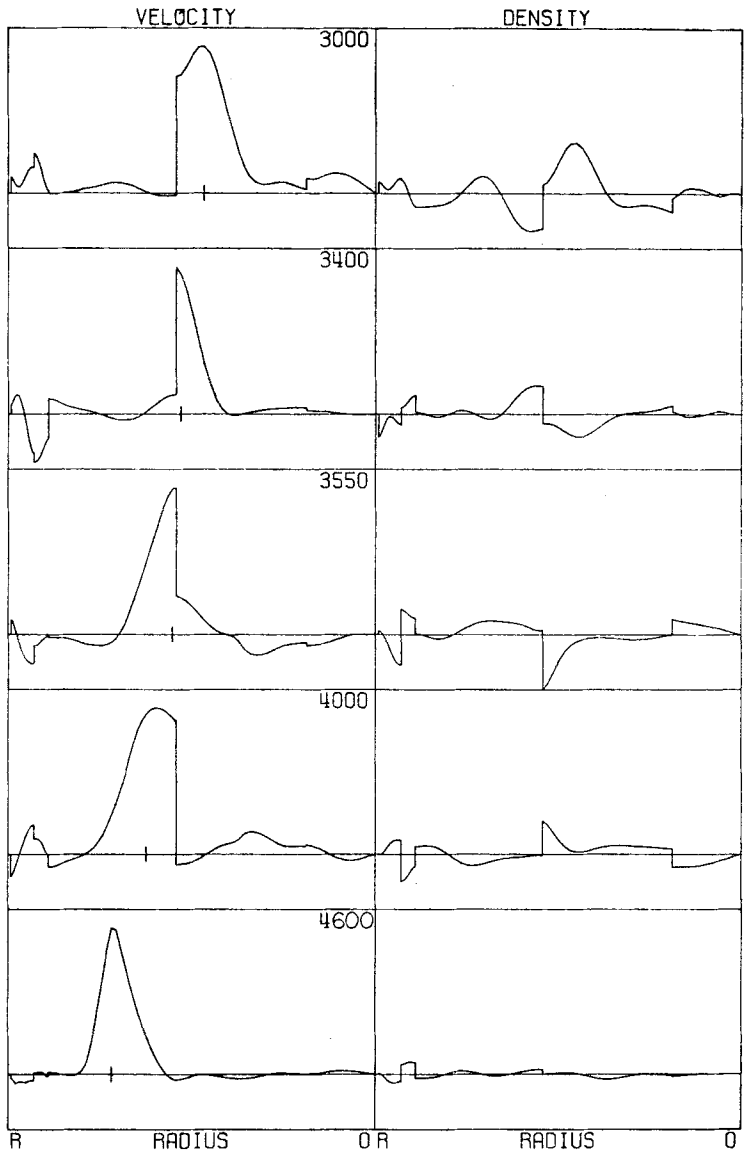

FIG. 4(a) continued. See caption on page 428.

concentrated in the central peak or else the peak maxima are more than one-half peak width removed from the radius for which these kernels are computed. We conclude that the features of the density solution below 2400-km radius are poorly determined by the data, including the magnitude of the density jump at the Lehmann discontinuity. The other regions where the localizations of the averaging kernels are poor are the shear velocity in the inner core, where there is negative trade-off with density in the outer core, the shear velocity in the vicinity of 4000-km radius, where there is coupling with the density perturbation in the lower mantle and outer core, and the compressional velocity in the vicinity of 2400-km radius, above the point where P'_{AB} rays bottom.

The resolving power of the data sets for the velocities and density is particularly good near discontinuities, the exception being for density near the Lehmann discontinuity. For example, the resolving length for compressional velocity at 1400-km

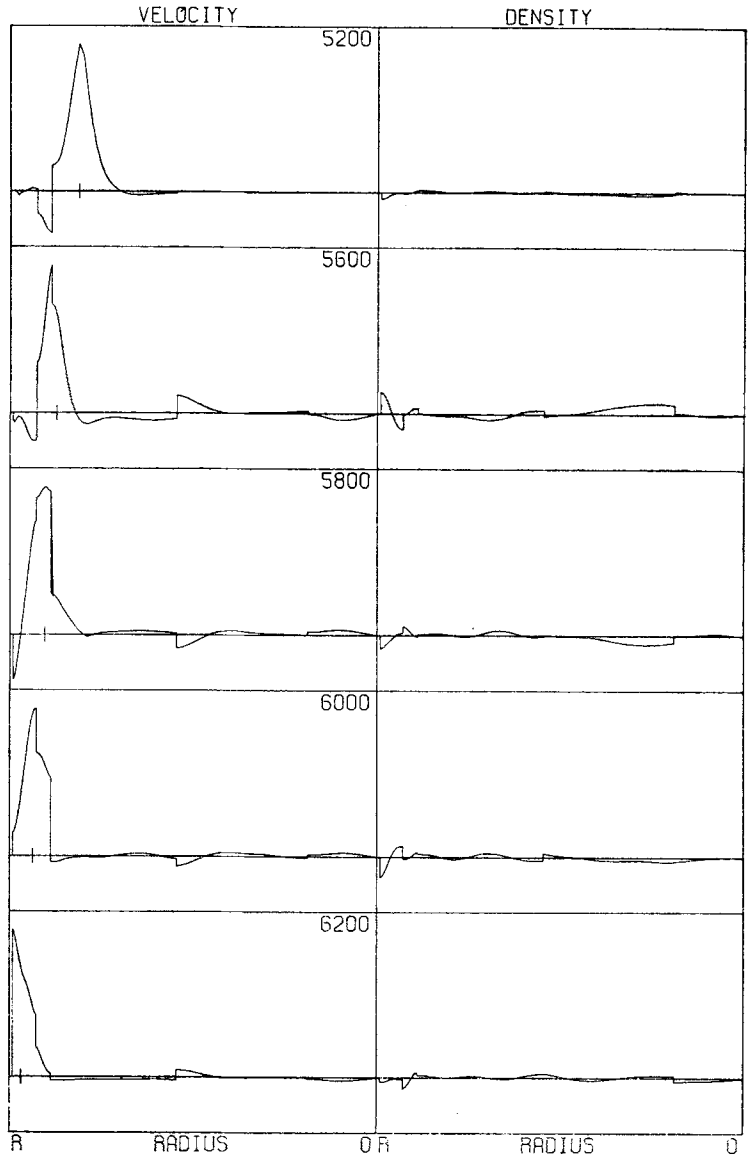

FIG. 4(a). Averaging kernels for compressional velocity perturbations at various r_0's computed with the shear velocity fixed. The radius r_0 is indicated by the number in the upper right-hand corner and by the vertical line. Kernels are computed using a data set consisting of the eigenperiods of the following modes and the differential travel times of the following phase combinations: ${}_{0-4}S_0$, ${}_0S_2$, ${}_0S_3$, ${}_0S_5$, ${}_0S_7$, ${}_0S_9$, ${}_0S_{12}$, ${}_0S_{15}$, ${}_1S_2$, ${}_1S_{7-10}$, ${}_2S_{1-4}$, ${}_2S_6$, ${}_2S_{15}$, ${}_3S_{2-9}$, ${}_3S_{11}$, ${}_4S_{1-10}$, ${}_5S_3$, ${}_6S_1$, ${}_6S_4$, ${}_6S_5$, ${}_7S_2$, ${}_7S_3$, ${}_7S_5$, ${}_8S_1$, ${}_8S_2$, $PcP-P$, $P'_{AB}-P'_{DF}$, $P'_{BC}-P'_{DF}$. The left-hand side of each kernel is the 'velocity part' and indicates how the compressional velocity difference is averaged to obtain $\delta v_p(r_0)$. The right-hand side is the 'density part' and indicates how the density difference is averaged to obtain $\delta v_p(r_0)$. For an ideal data set with perfect resolution the density part would be zero and the velocity part would consist of a delta function centred at r_0.

FIG. 4(b). See caption on p. 431.

radius is only 350 km. This behaviour near discontinuities, discussed by Backus & Gilbert (1968), results from the fact that the Fréchet kernels are generally discontinuous at these radii. We enhance this behaviour by choosing an autocorrelation operator for the solution that is also discontinuous at these radii.

The region of highest resolution is the upper mantle shear velocity distribution. The averaging lengths for this region are about 200 km for the error level we have chosen. Primarily responsible for this resolving power are the well-determined periods of the fundamental spheroidal and toroidal modes and the differential times of $ScS-S$. Without this body-wave data to constrain the shear velocity in the lower mantle, the modes have much poorer resolution, and there is a strong coupling between the shear velocity and density perturbations. The pronounced shear low-velocity zone introduced by the inversion is a resolvable feature of model B1. Also resolvable is the relatively high (4·8 km s^{-1}) shear velocity above this zone. Between

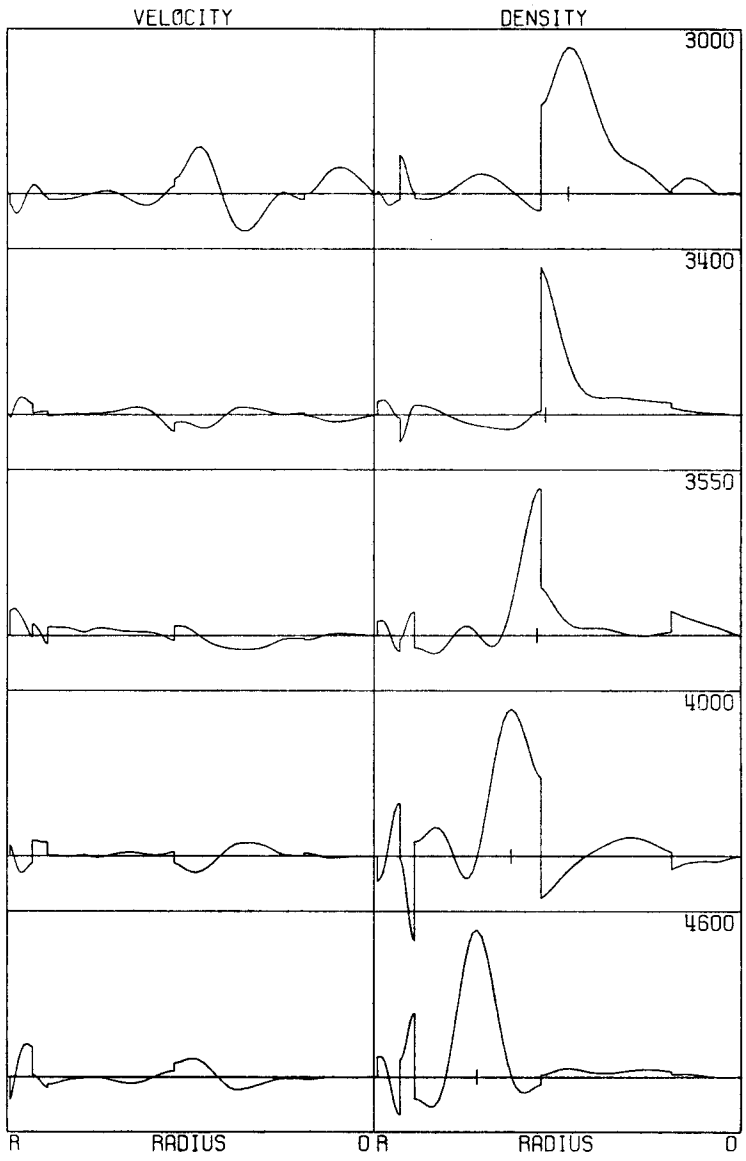

FIG. 4(b). continued. See caption on p. 431.

the discontinuities at 5700 km and 5951 km, B1 is characterized by a negative shear velocity gradient. The resolving lengths for this region are on the order of 400 km, about the same as the scale length of this feature, and it is only marginally resolvable. However, it is interesting to note that Ibrahim & Nuttli (1967) and Anderson & Julian (1969) using an independent set of absolute travel times have presented models with negative gradients in this region. Anderson & Julian (1969) discuss the mineralogical significance of this observation.

Although some of the details may be in doubt, the average perturbation to shear velocity in the upper mantle is well determined by the data we have used. An effect of this perturbation, which on the average is negative, is to increase the travel time of *S*-waves at 40° by about 3 s (*cf.* Section 8). The times of *S* at distances greater than 50° are further increased by the negative perturbation to shear velocity in the lower mantle. This negative perturbation has a scale length several times the peak widths

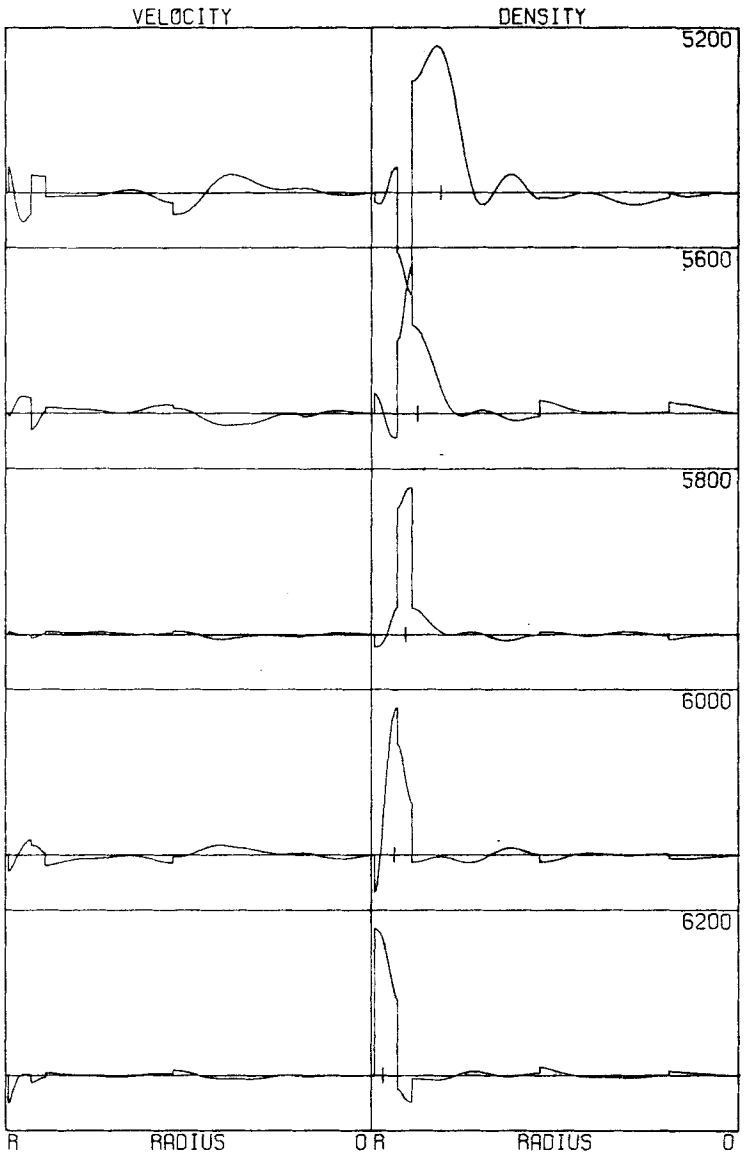

FIG. 4(b). Averaging kernels for density perturbations at various r_0's computed with the shear velocity fixed. The format of the figure and data set used is the same as in Fig. 4(a). In this case, the density part (R.H.S.) indicates how the density difference is averaged to obtain $\delta\rho(r_0)$, and the velocity part (L.H.S.) indicates how the velocity difference is averaged to obtain $\delta\rho(r_0)$.

of the appropriate averaging kernels, and, although some coupling with the density perturbations exists, this decrease in shear velocity seems to be required by the torsional oscillation data. For example, the calculated period of ${}_0T_3$ for B1 is 1702·43 s, *vs* the average observed period of $1705{\cdot}83 \pm 2{\cdot}529$ s (Dziewonski & Gilbert 1972). This yields a residual of $-3{\cdot}40$ s, greater than the standard error but within the 95 per cent confidence interval ($\pm 5{\cdot}47$ s) for this mode. Deleting the negative perturbation to shear velocity in the lower mantle, which would make B1 consistent with the recent observations of *S*-wave travel times (Hales & Roberts 1970a), would decrease the

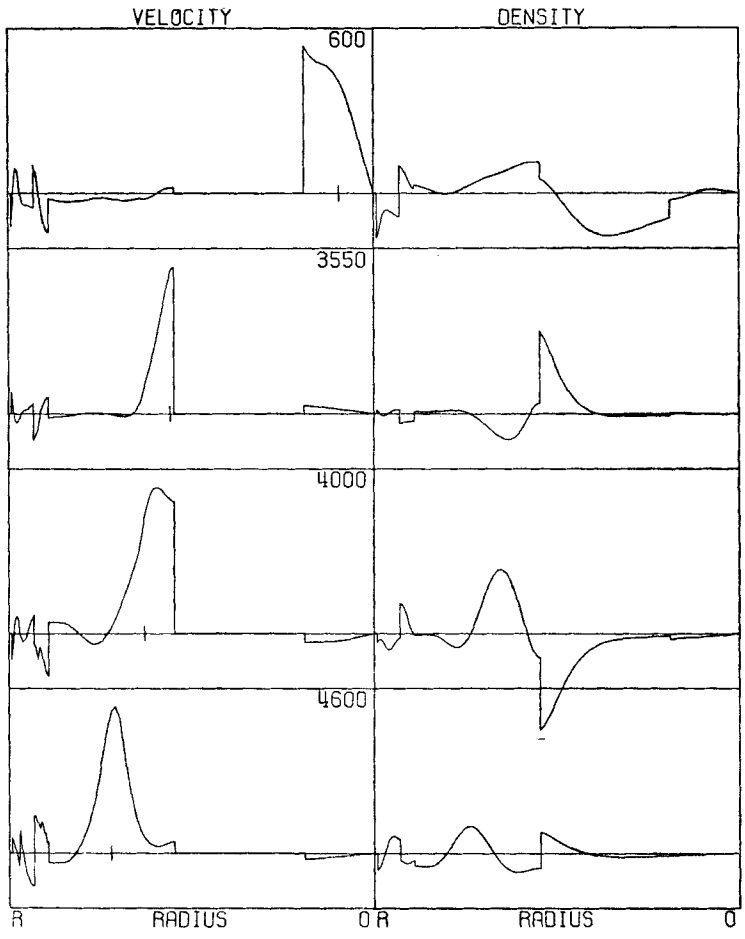

FIG. 4(c). See caption on p. 433.

calculated period by 4·38 s. This decrease is definitely inconsistent with the observations of ${}_0T_3$. The incompatibility of torsional oscillation periods and S-wave travel times was first pointed out by MacDonald & Ness (1961). However, there seems to be no significant incompatibility between the mode data and $ScS-S$ differential travel times, as evidenced by the good fit of model B1 to both of these data sets.

The perturbations to shear velocity in the inner core are very small, nowhere greater than 0·5 km s^{-1}, confirming the correctness of Dziewonski's & Gilbert's (1972) determination of 3·5 km s^{-1} as the mean velocity of this region. The high apparent velocity arrival seen at LASA by Julian, Davies & Sheppard (1972) and identified by them as $PKJKP$ implies, with this identification, a shear velocity in the inner core of about 2·9–3·0 km s^{-1}. This value seems to be incompatible with the mode data.

Unlike the results for shear velocity, no low compressional velocity zone is introduced in the upper mantle by the inversion. In this region the averaging kernels for compressional velocity are much broader than the corresponding kernels for shear velocity; the peak widths are generally greater than 500 km. Thus, the data we use do not resolve such a feature. However, the average perturbation in the upper mantle, which is negative and has a magnitude of about 0·07 km s^{-1}, is well determined. The positive perturbation to compressional velocity between the radii of 4900 and 5700 km can also be resolved. Acting together, these perturbations shift

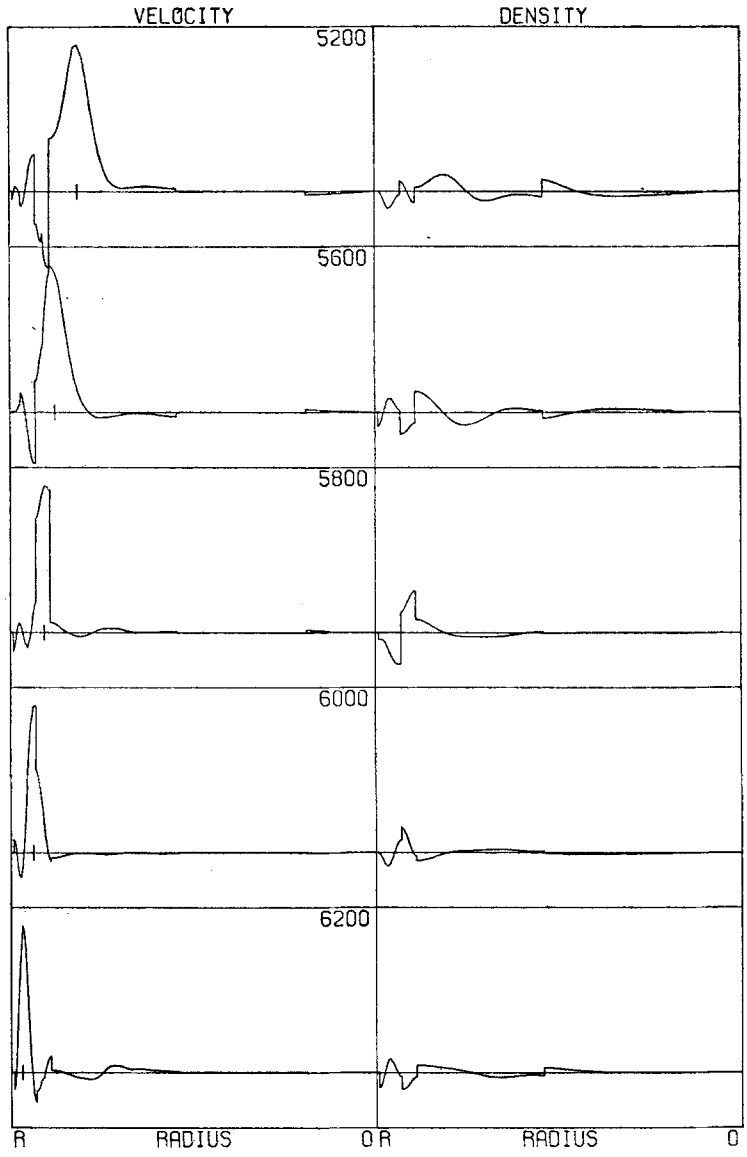

FIG. 4(c). Averaging kernels for shear velocity perturbations at various r_0's computed with the compressional velocity fixed. The format of the figure is the same as in Fig. 4(a) except the velocity is now the shear velocity. Kernels computed using a data set consisting of the differential travel times $ScS-S$ and the eigenperiods of the following modes: ${}_0S_2$, ${}_0S_3$, ${}_0S_{5-9}$, ${}_0S_{12}$, ${}_0S_{15}$, ${}_0S_{18}$, ${}_0S_{21}$, ${}_0S_{25}$, ${}_0S_{30}$, ${}_0S_{37}$, ${}_0S_{45}$, ${}_0S_{54}$, ${}_0S_{63}$, ${}_1S_2$, ${}_1S_4$, ${}_1S_5$, ${}_1S_{7-10}$, ${}_1S_{14-17}$, ${}_2S_2$, ${}_2S_{8-14}$, ${}_3S_{4-11}$, ${}_4S_{1-3}$, ${}_4S_{10}$, ${}_5S_2$, ${}_8S_2$, ${}_0T_{3-6}$, ${}_0T_8$, ${}_0T_{10}$, ${}_0T_{11}$, ${}_0T_{13}$, ${}_0T_{16}$, ${}_0T_{21}$, ${}_0T_{23}$, ${}_0T_{25}$, ${}_0T_{29}$, ${}_0T_{35}$, ${}_0T_{41}$, ${}_0T_{46}$.

the baseline for teleseismic P-waves by about $+0{\cdot}8$ s with respect to the starting model (and, therefore, with respect to the 1968 Seismological Tables for P) without disturbing the times of $PcP-P$.

The perturbation to compressional velocity in the outermost several hundred kilometres of the core is negative with a maximum absolute value of $0{\cdot}08$ km s^{-1} at the core–mantle boundary. The value of the velocity at the top of the core for model

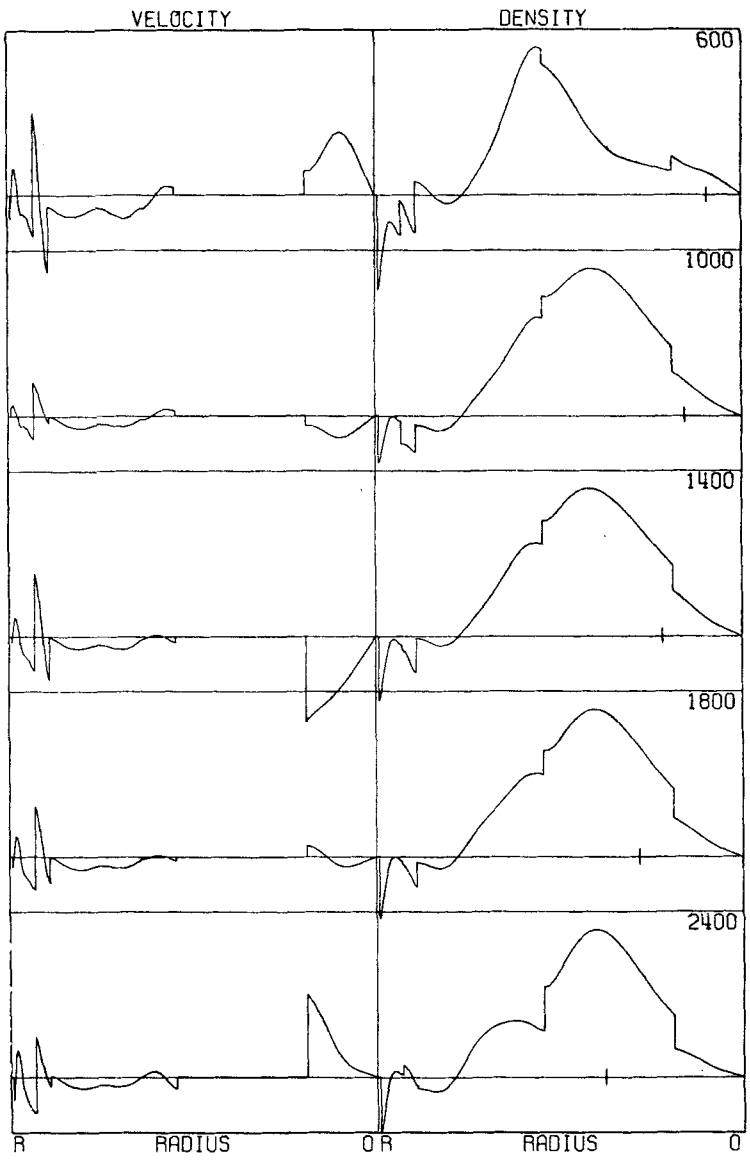

FIG. 4(d). See caption on p. 436.

B1 is 8·02 km s^{-1}, in agreement with Hales' & Roberts' (1971) conclusion that the velocities in this region are less than the values given by the Jeffreys–Bullen model. Their study was based on the observed differential travel times of $SKKS-SKS$. The computed times of $SKKS-SKS$ for B1 are listed along with the times computed from equation (3) of their paper in Table A4. Although this data was not used in the inversion, we note that the agreement is excellent. Evidently, the information contained in these data is also present in the higher spheroidal overtones.

Below a radius of 3000 km, the perturbation to compressional velocity in the outer core is positive. This perturbation is characterized by two lobes centred at radii of 1600 km and 2600 km. As a result the final model has a small ' kink ' in compressional velocity at 2600-km radius and a region of low gradient between the Lehmann discontinuity and 1600-km radius. The averaging kernels in this region have peak widths less than 1000 km, and these features appear to be real. If so, the outer core appears to

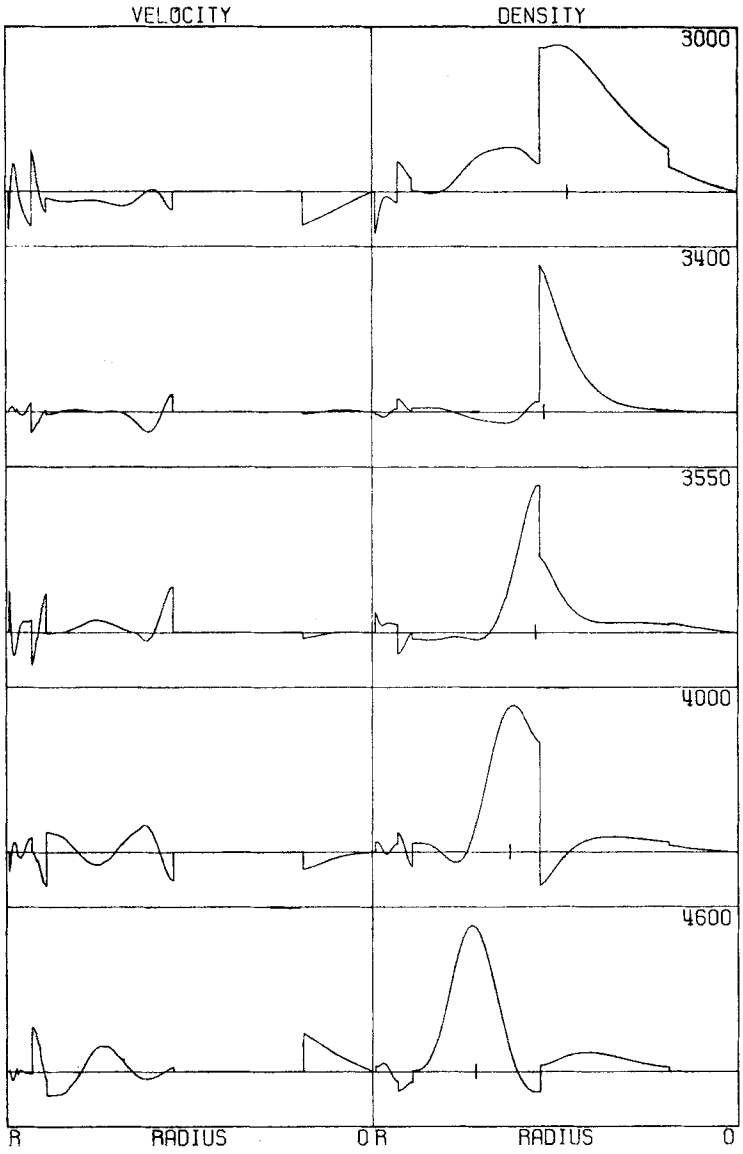

FIG. 4(d) continued. See caption on p. 436.

be inhomogeneous. However, some caution is justified, because, as we commented earlier, the localization of the kernels in the vicinity of 2400 km is poor. The perturbations to compressional velocity in the inner core are negligible, and the data functionals are not significantly affected if the velocity in this region is taken to be a constant 11·20 km s^{-1}.

For model B1, the average density in the upper 400 km of the mantle is 3·42 g cm^{-3}, about 0·06 g cm^{-3} less than the starting model. Since the peak widths of the averaging kernels are about 400 km in this region, averages over lengths less than this value are not well resolved. Thus, one cannot discuss with any useful precision the density of the 50–100 km-thick lithosphere. Between the discontinuities at 5700- and 5951-km radius the perturbation is again negative. The density perturbation is nearly a constant +0·05 g cm^{-3} throughout the entire lower mantle. The averaging widths are on the order of 1000 km, about half the dimension of this region. In the

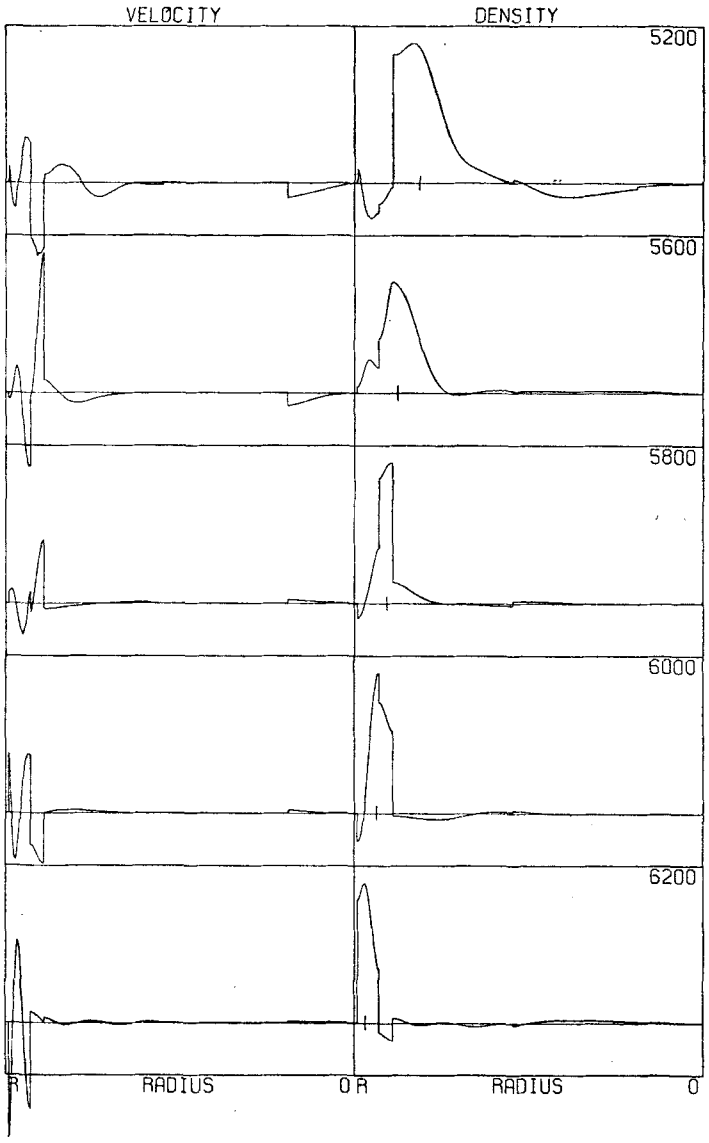

FIG. 4(d). Averaging kernels for density perturbations at various r_0's computed with the compressional velocity fixed. The format of the figure and the data set used is the same as in Fig. 4(c).

outer core the perturbation is negative with an average magnitude of 0·09 g cm^{-3}. Although the density kernels are quite localized in the outermost core with peak widths as short as 700 km, the localization of the averaging deteriorates rapidly below a radius of 2400 km, and the density distribution in this region of the Earth is somewhat uncertain.

7. Fit of Model B1 to the data

In this section we examine the fit of model B1 to the normal mode and the differential travel-time data.

Normal mode data

The mean eigenperiods and standard errors in the means taken from Tables 2 and 3 (all data) and Tables 4 and 5 of Dziewonski & Gilbert (1972) are given in Tables A1 (spheroidal modes) and A2 (toroidal modes) of this paper, along with Derr's (1969b) averages for ${}_0S_2$, ${}_0S_3$, and ${}_0T_2$ and Dziewonski's (1971, Table 3) values for ${}_0S_{51}$ through ${}_0S_{63}$. Also listed are the computed periods for model B1 and the relative errors of this model with respect to the data (computed minus observed/observed).

The quality of the overall fit is remarkable. Of the 123 spheroidal modes computed for B1, 74 or 60 per cent fit the data to 5 parts in 10 000, and 100 or 80 per cent fit to 1 part in 1000. Of the 54 toroidal modes, B1 fits 15 or 28 per cent to 5 parts in 10 000, and 33 or 61 per cent to 1 part in 1000. Only four of the modes calculated for B1 (${}_4S_1$, ${}_8S_2$, ${}_0T_2$, ${}_0T_{42}$) deviate from the observed by as much as 0·3 per cent.

The fit can be more properly evaluated by comparing the model-data residuals with the observational error estimated from the scatter in the data. Fig. 5 is a histogram giving the distribution of normalized residuals (computed minus observed divided by standard error in the mean). Although this histogram is fairly symmetric about zero, only 67 per cent of the modes fall within the interval $\pm 2\sigma$, and only 40 per cent fall within $\pm 1\sigma$, whereas the values expected for errors sampling a normal distribution with zero mean and known variance are 95 and 67 per cent, respectively. Of course, the sample variances are only estimates of the true variances. To account for this we have computed the symmetric 95 per cent confidence intervals associated with the observations using Student's method (Freeman 1963). These intervals are listed in Tables A1 and A2. For model B1, 70 per cent of the computed spheroidal modes

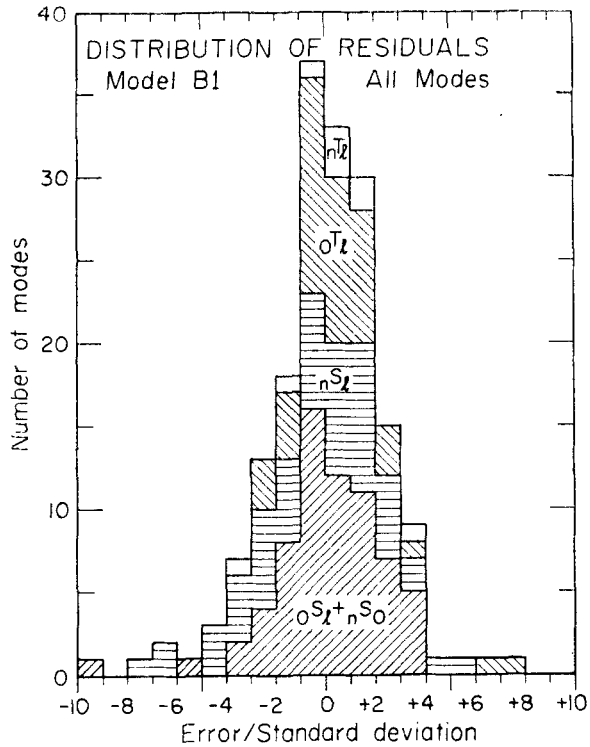

FIG. 5. Histogram showing the distribution of residuals for the mode data used in the inversion. All the residuals have been normalized by the standard errors in the means associated with the data.

and 81 per cent of the computed toroidal modes fall within the 95 per cent confidence intervals for the data. Both of these figures are significantly less than the 95 per cent expected, so we conclude that either B1 is not as good a fit to the data as it might be or the assumptions related to the distribution of errors (independent and normal with zero mean) are not correct.

Some evidence suggests that this disagreement is due in part to contamination of the observations by adjacent modes. Dziewonski & Gilbert (1972) have discussed the problem of mode contamination for this data set. They point out that the mean observed eigenperiods of ${}_0S_{10}$, ${}_0S_{14}$, ${}_0S_{20}$, ${}_1S_6$, ${}_3S_3$, and ${}_3S_{10}$ may be biased. In each case the periods of these modes computed for B1 lie outside the 95 per cent confidence intervals for the data.

Table 2 is a list of the 32 modes with periods greater than 300 s which are not fit within their 95 per cent confidence intervals by model B1. Nineteen of the 25 misfit spheroidal modes and four of the seven misfit toroidal modes have eigenperiods in close enough proximity to other modes to make their identification difficult. The modes that possibly contaminate the observations and their theoretical eigenperiods are also given in Table 2. If these 23 modes are deleted, 87 per cent of the remaining spheroidal modes with periods exceeding 300 s lie inside the 95 per cent confidence intervals, as do 93 per cent of the toroidal modes.

We have plotted the relative differences between B1 eigenperiods and the Dziewonski–Gilbert observations for the fundamental mode in Figs 6 (spheroidal modes) and 7 (toroidal modes). The highly discrepant modes (such as ${}_0S_{10}$, ${}_0S_{20}$, ${}_0S_{32}$, ${}_0S_{41}$, ${}_0S_{44}$, ${}_0T_7$, ${}_0T_{17}$, and ${}_0T_{37}$) appear on this plot as isolated 'tears' in the residuals. The effects of these isolated errors may be suppressed by smoothing (but this, of course, removes the independence of the individual observations). Dziewonski *et al.* (1972) smoothed the free oscillation data used by Dziewonski & Gilbert (1972) and we have plotted these as B1 residuals in Figs 6 and 7. Smoothed free oscillation values, based on earlier data, have also been tabulated by Haddon & Bullen (1969). The smoothed values are generally more consistent with model B1. For example, the average absolute error for B1 relative to the raw fundamental spheroidal mode data is 0·043 per cent for periods between 187 and 812 (${}_0S_7 - {}_0S_{47}$). This is reduced

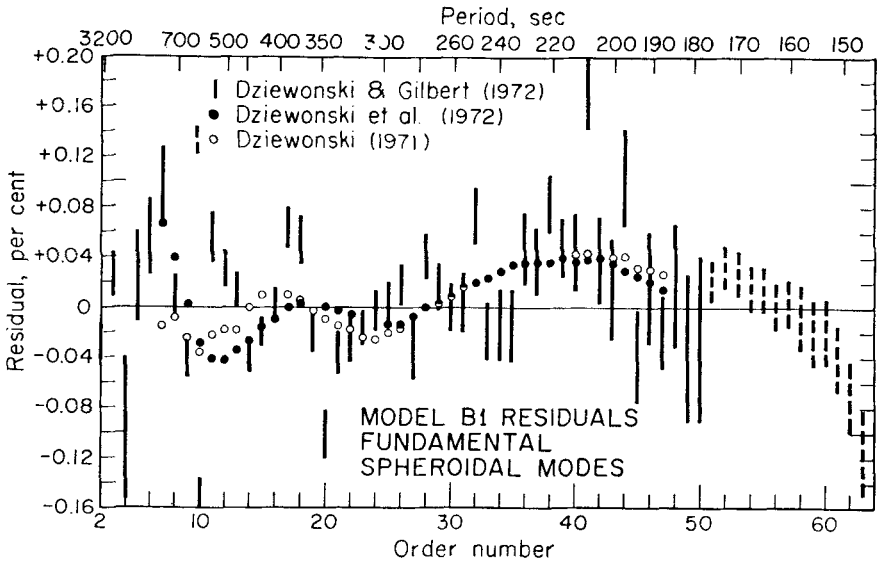

FIG. 6. Fundamental spheroidal mode data plotted as residuals with respect to model B1. Error bars represent standard errors in the mean.

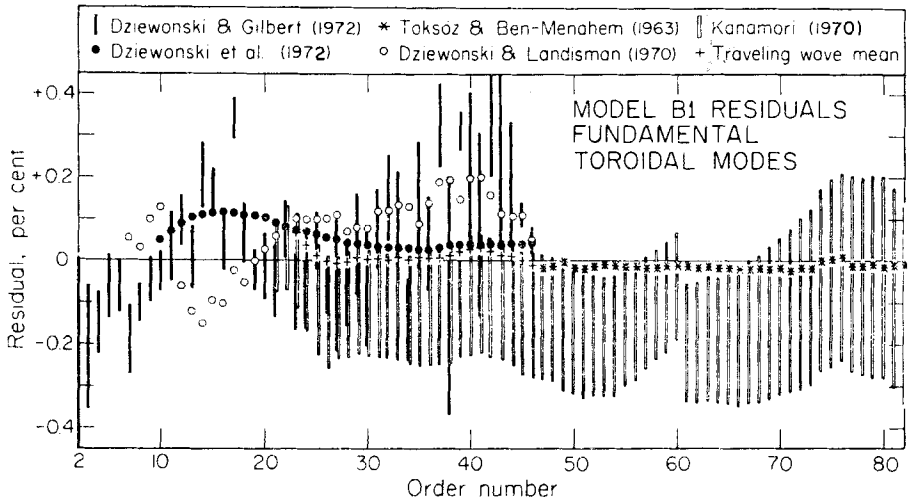

FIG. 7. Fundamental toroidal mode data plotted as residuals with respect to model B1. Error bars represent standard errors in the mean.

to 0·024 per cent when the smoothed values of Dziewonski, Mills & Bloch (1972) are used. Similarly, the average residual for B1 relative to the raw fundamental toroidal mode data is 0·12 per cent for periods between 177 and 619 s (${}_0T_{10} - {}_0T_{46}$) and 0·06 per cent relative to the smoothed data. The discrepancies between the raw and smoothed eigenperiods for the fundamental modes are possibly due to adjacent peak contamination.

In cases where the group velocities of the interfering modes are well separated, the travelling wave method can be used to avoid interference. A particularly careful study of the eigenperiods between 300 and 150 s has been done by Dziewonski & Landisman (1970) using the travelling wave method. Results for the torsional oscillation have also been given by Toksöz & Ben-Menahem (1963) and Kanamori (1970) for composite paths. These have been plotted in Figs 6 and 7 along with the raw and smoothed values obtained by the standing wave method. For the spheroidal modes the agreement between the smoothed eigenperiods and those derived by the travelling wave method is quite good. For torsional oscillations there are differences among the various studies. For example, in the range for which they overlap, the values given by Dziewonski & Landisman (1970) and Kanamori (1970) deviate systematically by about 0·2 per cent. Evidently, these discrepancies are due to path differences and reflect the fact that the fundamental toroidal modes are more sensitive to lateral variations in the upper mantle and are less readily measured due to lower Q than the fundamental spheroidal modes. The Dziewonski–Landisman values have positive residuals with respect to B1, whereas the residuals for Kanamori's (1970) are negative. We have combined their observations and have plotted the average as the ' travelling wave mean ' in Fig. 7. Over the period range 177–346 s (${}_0T_{21} - T_{46}$) the average B1 residual for the travelling wave means is less than 0·02 per cent. The agreement with the Toksöz–Ben Menahem (1963) data in the period range 104–174 seconds is equally good, certainly within the precision of this data.

Some of the disagreement between B1 and the mode data appears to be real. In particular, the fit to the modes ${}_1S_4 - {}_1S_{10}$ is poor. These modes are sensitive to the properties near the core–mantle boundary, and the misfit may indicate that B1 needs some slight modification in this region.

The fit of model B1 to the normal mode data seems to be as good or better than the fit of other published Earth models. It is a bit difficult to make a complete

Table 3

The number and percentages of eigenperiods with periods greater than 300 *s that are fit by various recent models. A mode is considered fit if its theoretical period lies within the* 95 *per cent confidence interval for the datum. Models UTD*124 *A and B are from Dziewonski & Gilbert* (1972)*; model* HB_1 *is from Bullen & Haddon* (1969)*; Wang's model is from Wang* (1968)*; Press'* (1970) *model is a 'typical' Monte Carlo model*

Modes		B1	UTD 124A	UTD 124B	HB_1	Wang (1972)	Press (1970)
Radial modes	# computed	4	4	4	4	4	1
	# fit	4	2	2	1	2	1
	% fit	100	50	50	25	50	100
Fundamental	# computed	23	23	23	23	23	21
spheroidal	# fit	16	7	5	6	9	2
modes	% fit	70	30	22	26	39	10
Spheroidal	# computed	45	45	45	45	33	8
overtones	# fit	27	25	29	17	16	1
	% fit	60	56	64	38	49	13
Fundamental	# computed	23	23	23	23	23	20
toroidal	# fit	18	19	17	19	10	5
modes	% fit	78	83	74	83	44	25
Toroidal	# computed	9	9	9	9	6	0
overtones	# fit	7	7	8	2	1	—
	% fit	78	78	89	22	17	—
TOTALS	# computed	104	104	104	104	89	50
	# fit	72	60	61	45	38	9
	% fit	69	58	59	43	43	18

Table 4

Observed and theoretical group velocities for the fundamental modes. Data from Dziewonski et al. (1972). *Model* 5·08*M is described by Kanamori & Press* (1971)

Mode	T (s)	U_{B1} (km s^{-2})	U_{obs} (km s^{-2})	Residual (km s^{-1}) B1	5·08 M
${}_0S_9$	633·69	6·263	6·264	−0·001	—
${}_0S_{12}$	502·34	5·002	5·011	−0·009	—
${}_0S_{15}$	426·16	4·534	4·535	−0·001	+0·008
${}_0S_{25}$	297·72	3·723	3·725	−0·002	+0·013
${}_0S_{29}$	268·49	3·617	3·623	−0·006	+0·005
${}_0S_{31}$	256·12	3·591	3·596	−0·005	+0·004
${}_0S_{34}$	239·67	3·574	3·575	−0·001	+0·002
${}_0S_{38}$	220·80	3·576	3·574	+0·002	−0·005
${}_0S_{40}$	212·43	3·583	3·581	+0·002	−0·011
${}_0S_{44}$	197·40	3·605	3·598	+0·007	−0·012
${}_0S_{47}$	187·40	3·626	3·611	+0·015	−0·011
${}_0T_{10}$	618·84	5·011	5·072	−0·061	—
${}_0T_{11}$	574·82	4·901	4·957	−0·056	—
${}_0T_{13}$	505·02	4·738	4·759	−0·021	—
${}_0T_{16}$	429·40	4·586	4·579	+0·007	+0·015
${}_0T_{21}$	345·67	4·467	4·456	+0·011	+0·012
${}_0T_{23}$	320·98	4·444	4·441	+0·003	+0·001
${}_0T_{25}$	299·66	4·429	4·426	+0·003	−0·002
${}_0T_{29}$	264·64	4·413	4·423	−0·010	−0·020
${}_0T_{35}$	225·24	4·406	4·426	−0·020	−0·036
${}_0T_{41}$	196·05	4·407	4·422	−0·015	−0·034
${}_0T_{46}$	176·93	4·411	4·420	−0·009	−0·031

comparison, because many authors have not tabulated theoretical periods corresponding to all the modes for which data is now available. Table 3 attempts to show how well several of the more recent models fit the mode data. Listed are the numbers and percentages of modes with periods greater than 300 s that are fit by B1, UTD124A & B (Dziewonski & Gilbert 1972), HB_1 (Haddon & Bullen 1969), Wang's (1972) model, and Press' (1970) 'typical' Monte Carlo model. For the purpose of compiling this table, a mode was considered 'fit' if its theoretical period fell within the 95 per cent confidence interval computed for the datum. (The confidence intervals we used can be found in Tables A1 and A2.) On the basis of this comparison, B1 is superior to the other models. With the exception of the fundamental spheroidal mode data, models UTD124A & B are also excellent fits. Dziewonski & Gilbert (1972) point out that the fit of model HB_1 to the spheroidal overtone data is improved by introducing a non-zero shear velocity in the inner core. As it stands, HB_1 is a very good fit to the fundamental toroidal mode data. Wang's model is not a bad fit to the spheroidal mode data, but, for the toroidal eigenperiods the model-data residuals are systematically positive with magnitudes of 0·1–0·4 per cent. Only 44 per cent of these data are fit by this model, compared with 83 per cent for UTD124A and HB_1 and 78 per cent for B1. Press' model is a poor fit to both the toroidal and spheroidal mode data, but this is understandable: in his Monte Carlo searches he assigned 0·4 per cent tolerances to all eigenperiods except the period of ${}_0S_0$.

Average group velocity data, compiled from great circle dispersion studies, have been tabulated by Kanamori (1970) and Dziewonski *et al.* (1972). We did not use any group velocities to derive model B1, but this kind of data does provide a useful check on upper mantle structure. Table 4 lists the theoretical group velocities computed from two models, model B1 and model 5·08M of Kanamori & Press (1970), along with the observed values given by Dziewonski *et al.* (1972). Model 5·08M is one of Press' Monte Carlo solutions specifically modified to better agree with group velocity data. Both models staisfy the Kanamori data set within its rather large errors. The technique used by Dziewonski *et al.* (1972) does not yield estimates of the uncertainties, but we see from the table that the overall fit of both models is quite good. Model B1 fits the Rayleigh wave data with an average relative error of 0·1 per cent and the Love wave data with an error of 0·4 per cent.

Differential travel times

The differential travel times computed for model B1 are compared with the data used in the inversion in Table A3 of the Appendix. Also appearing in this table are the standard errors in the means and the 95 per cent confidence intervals computed for the data. Thirty of the 39 differential travel times fit within their 95 per cent confidence intervals, and only 4 of the model-data residuals exceed one second. The largest, for $ScS-S$ at 30°, is −3·0 s.

Most of the large residuals are explained by bias or internal inconsistency in the data, For example, the residual for $ScS-S$ at 40° is −1·1 s, exceeding the standard error, but within the 95 per cent confidence interval of the datum. The large error reflects the fact that it is difficult to observe $ScS-S$ times near 40° due to the presence of the interfering phases *sS* and *SS*. The times computed for $P'_{BC}-P'_{DF}$ at distances greater than 153° lie outside the 95 per cent confidence intervals for the data. However, the raw data show a considerable increase in their scatter at distances greater than 153° (Jordan 1972). This behaviour may indicate that the point C of the *PKP* curve is nearer to 153° than it is to 158°, the distance of this turning point computed from model B1.

Other sets of differential travel-time data that can be used for gross Earth modelling are the $SKS-S$ and $SKKS-SKS$ times given by Hales & Roberts (1970a, 1971). These are given at 5° intervals in Table A4, along with the times computed for B1.

B1 is an excellent fit to the $SKKS-S$ data and an adequate fit to the $SKS-S$ data. Since we did not use these times in the inversion, the good agreement suggests that the information they contain is duplicated in the eigenperiod and differential travel-time data we did use.

8. Comparison with absolute travel times

Although no absolute travel times were used to obtain model B1, comparision of the theoretically predicted times with the observed data is of considerable interest. Because source and receiver locations are not uniformly distributed over the Earth, oceanic provinces being particularly poorly sampled, one does not necessarily expect agreement between model predictions and experimental travel times. In a gross way, any discrepancies should be measures of differences between the average Earth and some sort of 'oceanic deficient' representation that is sampled by presently available absolute travel-time data.

The absolute travel times at various distances for the phases *P*, *S*, *PcP*, *ScS*, *PKP* or *P'*, and *PKiKP* computed from model B1 are listed in Tables A5–A9. For comparison we have also listed the J–B times for each of these phases except *PKiKP*, the times of *P*, *PcP*, and *PKP* from the 1968 Seismological Tables for *P* (Herrin *et al.* 1968), the times of *PKiKP* from Engdahl, Flinn & Romney (1970), and Hales' & Roberts' (1970) times for *S*. For the *P* and *S* phases, $dT/d\Delta$'s are listed.

P times

Model B1 has *P*-wave residuals that average 0·8 s late relative to the 1968 Seismological Tables for *P* (Herrin *et al.* 1968) over the distance range 30°–90°. This residual curve is shown in Fig. 8. The residual varies from +1·4 s at 30° to +0·7 s at 90°. Thus, there is a tilt as well as an offset. The data of Kogan (1960), Carder, Gordon & Jordan (1966), Cleary & Hales (1966), Muirhead & Cleary (1969), and Enayatollah (1971) support both the offset and the tilt. The results of these studies, along with the travel times of Lomnitz (1971), are plotted as residuals in Fig. 8.

In comparing model times with observations, the studies of Kogan (1960) and Muirhead & Cleary (1969) are particularly relevant because they used oceanic sources (explosions in the South Pacific) and continental stations and are more pertinent to average Earth studies than explosions in Nevada and the Aleutians. The average residual for Marshall Island events between 30° and 90° is +0·8 s, the same as for

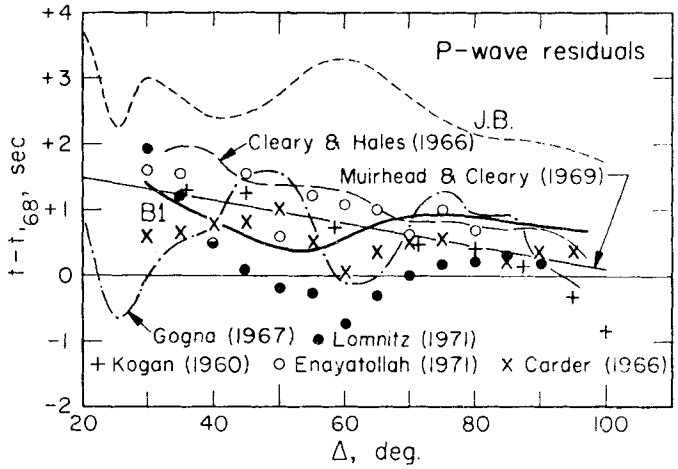

FIG. 8. *P*-wave travel times (surface focus) as residuals with respect to the 1968 Seismological Tables for *P* (Herrin *et al.* 1968).

model B1. The Muirhead & Cleary (1969) data can also be used to estimate residuals as a function of distance. Between 30° and 50° the mean residual and standard deviation is $+0{\cdot}79 \pm 0{\cdot}71$ s, relative to the 1968 Tables. In this range the mean B1 residual is +0·86 s, in satisfactory agreement. Between 50° and 70° the Muirhead–Cleary residual is $0{\cdot}78 \pm 0{\cdot}45$ s. Again the agreement is satisfactory; B1 has a mean residual of +0·62 s. Between 70° and 90° the observed residual is $+0{\cdot}35 \pm 0{\cdot}51$ s, versus a B1 residual of +0·86 s. Small or negative residuals beyond 80° are supported by the observations of Kogan (1960), Carder *et al.* (1966), and Lomnitz (1971). Since the B1 residual is positive, this may indicate that the lowermost 300 km of the mantle has higher compressional wave velocities than those given by model B1.

We note, however, that the $dT/d\Delta$ of *P*-waves at the geometrical shadow boundary (98·5°) computed from B1 using geometrical ray theory is 4·45 s/deg, considerably lower than the 4·56 s/deg found by Herrin *et al.* (1968). A value of 4·56 s/deg has also been measured along the AB branch of the P4KP travel-time curve by Adams (1972). A straightforward interpretation of this data using geometrical ray theory implies that the *P* velocity at the base of the mantle is lower than that given by B1. Indeed, it is possible to explain both the measured travel times and $dT/d\Delta$'s by introducing a low-velocity layer at the base of the mantle. This seems premature, however, since geometrical ray theory is an inadequate description of wave propagation in this region (Johnson 1969; Richards 1973). Richards (1973), for example, has suggested that the high apparent velocities measured along the AB branch of P4KP are due to tunnelling of mantle rays into the core and can be explained by a Jeffreys-type velocity structure, such as model B1.

PcP times

The times of *PcP* are controlled by both the compressional velocity in the mantle and the radius of the core. Model B1 times are early with respect to J–B times by 1·5–3·5 s, in general agreement with times measured from nuclear explosions. Fig. 9 shows J–B residuals for B1 and the 1968 Tables, as well as the observational results of Kogan (1960), Taggert & Engdahl (1968), and Bolt, Niazi & Somerville (1970). Both B1 and the 1968 Tables agree to within the stated experimental uncertainties. (Of course, the times of *PcP* given in the 1968 Tables were derived from Taggart & Engdahl's (1968) data.) However, because B1 *P* times are somewhat greater than the 1968 Tables, a slightly larger core radius, 3485 km, is required.

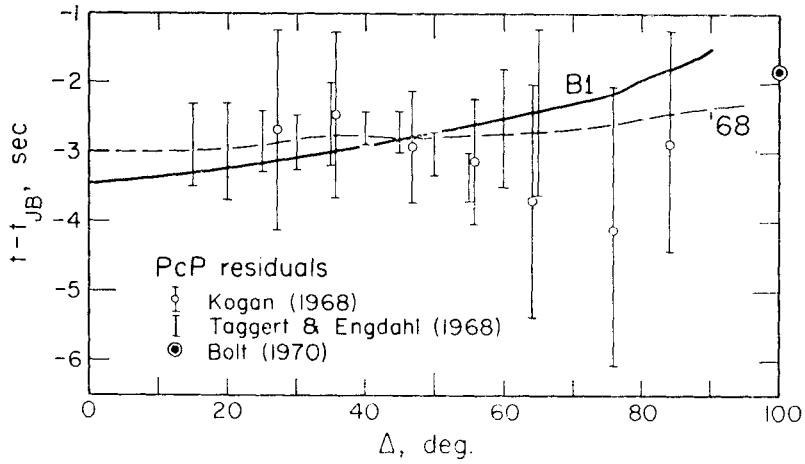

FIG. 9. *PcP* travel times (surface focus) plotted as residuals with respect to the 1940 Jeffreys–Bullen Tables.

Times of core phases

The *PKP* (or *P'*) travel-time curve (surface focus) for model B1 is shown in Fig. 10, along with Bolt's (1968) times for the AB and DF branches which appear in the 1968 Tables. The fit to Bolt's times is good; the differences are generally less than one second. Fig. 11 shows P'_{DF} (*PKIKP*) residuals for model B1 and several other studies taken with respect to Bolt's times. The B1 residual curve has a positive slope at distances greater than 145°. This agrees with the observations of Gogna (1968) and Cleary & Hales (1970). At distances less than 145°, the B1 residual curve has a negative slope, whereas Gogna (1968) and Cleary & Hales (1970) indicate a positive trend. These times are sensitive to the details of the transition region between the

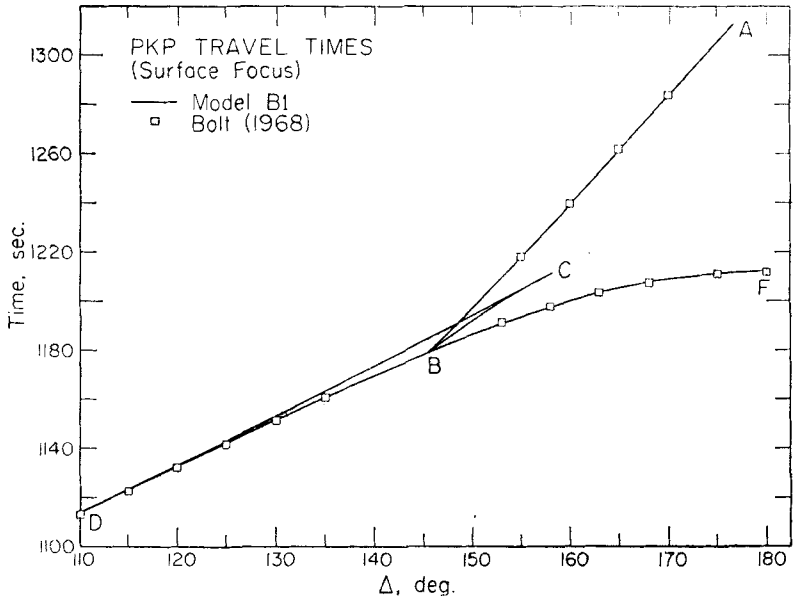

FIG. 10. The *PKP* travel-time curve (surface focus) for model B1.

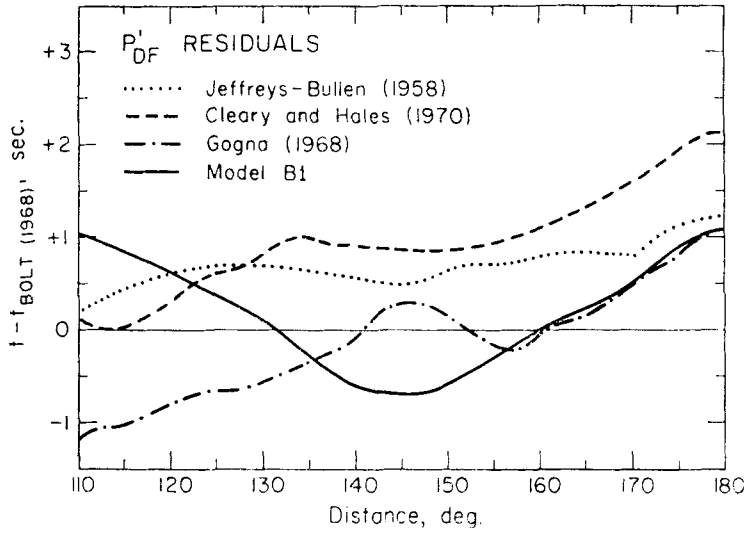

FIG. 11. P'_{DF} (or *PKIKP*) travel times (surface focus) as residuals with respect to the 1968 Seismological Tables for *P* (Bolt 1968).

inner and outer cores and may indicate that the radius of the Lehmann discontinuity is greater than the 1215-km value given by B1.

However, the absolute travel times most sensitive to the radius of the Lehmann discontinuity are those of *PKiKP* at short distances. A comparison of the times of *PKiKP* given by Engdahl *et al* (1970, Table 1) with those of model B1 is shown in Table A9. In the distance range 10° to 50°, B1 times are consistently earlier than the times given by Engdahl *et al.* (1970) by 0·7–0·5 s. Although the magnitudes of the differences are small and could be entirely explained by a difference in baseline, the comparison suggests, if anything, a slight decrease in the radius of the Lehmann discontinuity.

From Fig. 10, it can be seen that B1 predicts that the points A, B, C, and D of the *PKP* curve should occur at distances of 177°, 145°, 158°, and 111°, respectively. Jeffrey's distances for these cusps are 176°, 143°, 147°, and 110°. In a recent study of *PKP* amplitudes and $dT/d\Delta$'s, Whitcomb (1973) has obtained preliminary values of 167°, 144°, 154°, and 121° for the turning points, but, as he points out, his criterion for determining the distances of the points A and D (vanishing curvature) is subject to some error. D. Davies (private communication) suggests a distance of 156° for the point C, based on his observations of *PmKP* phases at LASA. The value of 145° given by B1 for the position of the B caustic is somewhat greater than Jeffrey's value of 143°. Shahidi (1968) has made a detailed study of *PKP* amplitudes in the vicinity of this caustic, and he puts the point B at 144·2° which is in good agreement with our model.

S *times*

S-wave residuals of model B1 with respect to the Jeffreys–Bullen Tables are shown in Fig. 12. At 40° the residual is +4·3 s and increases to +10·4 s at 95°. For comparison we have also plotted the results from Kogan (1960), Lehamann (1964), Ibrahim & Nuttli (1967), Doyle & Hales (1967), Cleary (1969), Hales & Roberts (1970a), and Bolt *et al.* (1970).

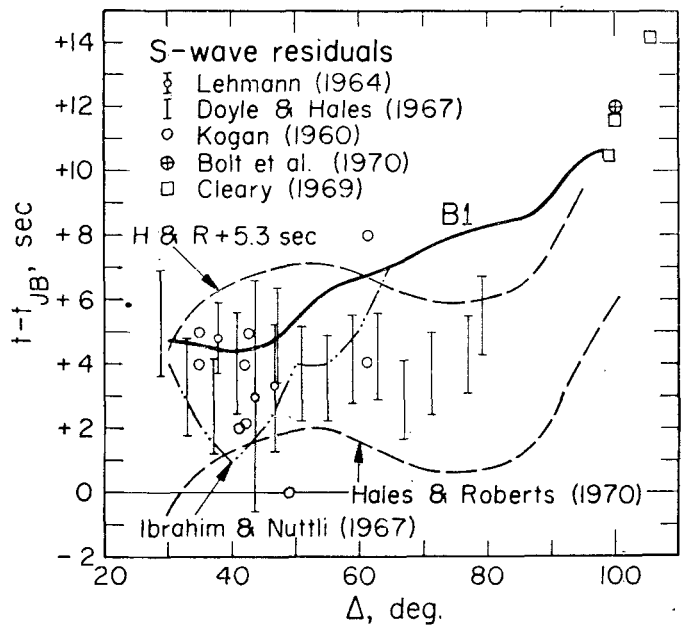

FIG. 12. *S*-wave travel times (surface focus) plotted as residuals with respect to the 1940 Jeffreys–Bullen Tables.

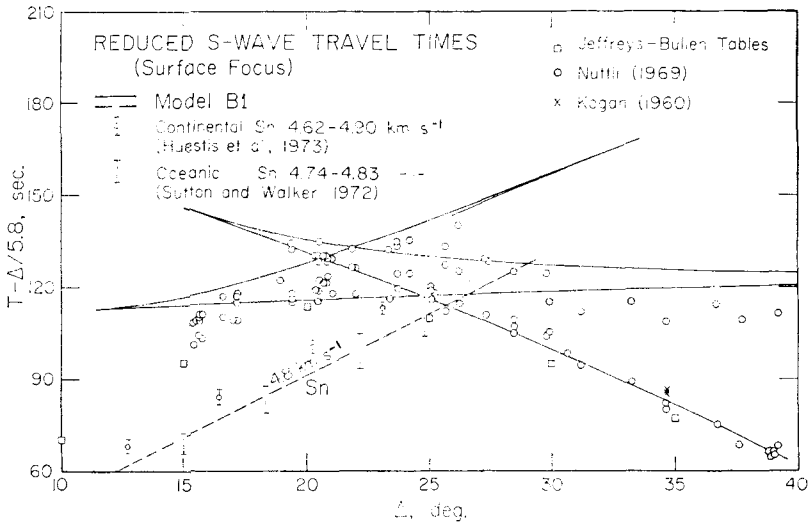

FIG. 13. The reduced *S*-wave travel-time curve (surface focus) for model B1 in the distance range 10°–40°. The reducing velocity is 5·8 km s^{-1}.

Since shear velocities are approximately half the magnitude of the compressional velocities and show greater variability in the upper mantle, the problem of baseline bias is especially acute for *S*-wave travel times. Doyle & Hales (1967), for example, have shown that *S* station anomalies have a range of 8 s for U.S. stations alone. Model B1 indicates that the average upper mantle is slower for *S*-waves than the J–B upper mantle by about 4 s. Kogan's (1960) work on *S* times from nuclear explosions in the South Pacific is concordant with this conclusion; in the distance range 30°–45° her times yield a positive residual of about 4 s. Lehmann (1964) studied European records of a Hindu Kush earthquake, and her results show a J–B residual of $+3{\cdot}5 \pm 3{\cdot}9$ s for the distance range 36°–50°.

A very crude baseline can also be established from the station and source residuals of Hales & Roberts (1970b). Their mean station residual is $-0{\cdot}33$ s, and their mean source residual is $+4{\cdot}63$ s. The mean path residual is $+4{\cdot}3$ s, and residuals for oceanic stations and sources are up to 3 s more positive. The Hales & Roberts curve in Fig. 12 is tied to Nevada sources and central U.S. stations and has a mean J–B residual of $+1{\cdot}2$ s. A further offset, or baseline shift, of $+5{\cdot}3$ s brings the mean residual of the Hales & Roberts data and model B1 into agreement and is generally consistent with the mean path residual computed above. The shifted Hales & Roberts curve is also plotted in Fig. 12.

Besides a shift of $+4$ to $+5$ s at distances less than 50°, the *S*-wave residual curve for model B1 generally has a positive slope, so that the J–B residual for B1 at 95° is $+10{\cdot}4$ seconds. This increase is compatible with the times of so-called ' diffracted *S* ' or ' diffracted *ScS* ' observed by Cleary (1969) and Bolt *et al.* (1970). The results from other *S*-wave studies are ambiguous. Doyle & Hales (1967) found no significant differences between their observed times and J–B times in the distance range 30°–80°, a possible baseline shift excepted. Ibrahim's & Nuttli's (1967) residuals, on the other hand, indicated a positive slope between 40° and 65°; in this distance range their residuals increased by about 6 s. The Hales & Roberts (1970a) study, though compatible with Doyle & Hales (1967) at distances less than 80°, shows an increase in J–B residual of about 7 seconds between 30° and 95°.

The *S*-wave travel-time curve for distances between 10° and 40° computed for model B1 is shown in Fig. 13. The high S_n velocity (4·8 km s^{-1}) given by the model is

consistent with the observations of Sutton & Walker (1972) for oceanic paths. Also plotted in Fig. 13 are Nuttli's (1969) times measured from explosion sources. The agreement is good for first arrivals throughout most of the distance range. The times of the back branches, which are sensitive to the details of the velocity structure in the upper mantle, are somewhat discrepant. However, the travel times through the upper mantle show strong lateral variations, and we do not expect these observations, which sample the upper mantle under the western and central United States, to represent a world-wide average.

10. Discussion

We have derived a spherically symmetric model of the seismic velocities and density, model B1, that is consistent with most available seismological data pertaining to the average radial variations of these properties. Model B1 fits the eigenperiod data as well as can be expected: 77 per cent of the periods computed for B1 differ from the observed by less than one part in one thousand. We suspect that many of the modes that show large residuals are biased by adjacent mode contamination. B1 reproduces the major features of the observed travel-time curves. It is a good fit to the differential travel-time data and, excepting baseline differences, agrees with the observed absolute times as well. For B1 the times of *P*-waves bottoming in the lower mantle average 0·8 seconds greater than the times given by the 1968 Tables but agree with more recent studies. At 40° the *S*-wave times are 4·3 s greater than J–B, and the residuals increase with distance, in general agreement with the studies of Hales & Roberts (1970a). Clearly (1969), Bolt *et al.* (1970), and Ibrahim & Nuttli (1967).

Without a more extensive analysis of the resolving power of the data set only a few positive statements can be made about the uniqueness of the present model. We believe that, since B1 is a good fit to the normal mode data and also satisfies a large body of travel-time data, it is close to the real Earth, fine structure excluded. Model B1 should serve as a useful standard model for further studies of fine structure and lateral variations.

Individual models are also useful in the following way: If one is entertaining a set of hypotheses about the Earth and if an Earth model embodying these hypotheses can be found that satisfies the data sufficiently well, then there is no reason to reject these hypotheses, assuming the model is acceptable on other grounds as well. For example, Press (1970, 1972) maintains that a density of $3{\cdot}5-3{\cdot}6\ \mathrm{g\,cm^{-3}}$ is characteristic of the uppermost mantle. We see from Table 1 that model B1 has an average density of only $3{\cdot}33\ \mathrm{g\,cm^{-3}}$ in the upper 200 km of the mantle. Since B1 is a good fit to the data pertaining to the upper mantle, including group velocity data, we conclude that we have no evidence to refute the hypothesis that this region has a density less than $3{\cdot}4\ \mathrm{g\,cm^{-3}}$, which is consistent with a pyrolite, peridotite or pyroxenite composition. Of course, this result applies to the spherically averaged Earth. Note that our argument does not rule out the *possibility* of a high-density upper mantle; it merely states that a high density is not required to satisfy the data. It should also be pointed out that Press could not have found a model close to B1 because of the parameterization (model point spacing and perturbation step size) and the *a priori* bounds placed on allowable models; B1 falls outside these bounds in several critical regions. He also terminated his searches at error levels which would be considered unacceptable in the present study.

A similar result holds for the hypothesis that the lower mantle is characterized by an Adams–Williamson density gradient. B1 shows no significant departure from Adams–Williamson type behaviour (homogeneity and adiabaticity) in region D', so that any postulates of non-adiabatic thermal gradients or compositional variation in this region cannot be founded solely on the density profile resulting from the inversion of presently available data. However, the shape of the velocity depth

functions does suggest that the lower mantle is slightly inhomogeneous. It is interesting to note that the density profile in the lower mantle is quite close to that given by Birch's (1964) Solution II.

On the basis of the compressional velocities in the outer core this region appears to be inhomogeneous. This suggests that radial convection is limited to only part of the outer core. The anomalous velocity gradients at the top and the base of the outer core can be explained in terms of compositional gradients resulting from the settling of solid iron particles. Because of the effect of pressure on eutectic phase equilibria relations, the amount of solid iron and the composition of the liquid on the liquidus vary with depth in the core. Mechanical considerations then serve to redistribute the iron. The net effect is to stabilize the core against thermal convection.

The velocity and density jumps at the inner core–outer core boundary are consistent with the inner core being the same composition, on the average, as the outer core.

Acknowledgments

The authors would like to thank Mr Martin Smith for the use of his free oscillation program and Dr Bruce Julian, who provided the travel-time routines. Dr Adam Dziewonski and Dr Freeman Gilbert kindly gave us their data prior to its publication. Mr J. Bernard Minster assisted with the computations. This research was supported by the Advanced Research Projects Agency of the Department of Defense and was monitored by the Air Force Office of Scientific Research under contract F44620–72–C–0087.

Seismological Laboratory,
California Institute of Technology,
Pasadena, California.

References

Adams, R. D., 1971. Early reflections of *P'P'* as an indication of upper mantle structure, *Bull. seism. Soc. Am.*, **58,** 1933.

Adams, R. D., 1972. Multiple inner core reflections from a Novaya Zemlya explosion, *Bull. seism. Soc. Am.*, **62,** 1063.

Adams, R. D. & Randall, M. J., 1964. The fine structure of the earth's core, *Bull. seism. Soc. Am.*, **54,** 1299–1313.

Alexander, S. S. & Phinney, R. A., 1966. A study of the core–mantle boundary using *P* waves diffracted by the earth's core, *J. geophys. Res.*, **71,** 5943–5958.

Alsop, L. E., 1963. Free spheroidal vibrations of the earth at very long periods, Part II, *Bull. seism. Soc. Am.*, **53,** 503–516.

Anderson, D. L., 1964. Universal dispersion tables, 1. Love waves across oceans and continents on a spherical earth, *Bull. seism. Soc. Am.*, **54,** 681–726.

Anderson, D. L., 1967a. A seismic equation of state, *Geophys. J. R. astr. Soc.*, **13,** 9–30.

Anderson, D. L., 1967b. Latest information from seismic observations, *The Earth's mantle*, ed. T. F. Gaskell, pp. 355–420, Academic Press, New York.

Anderson, D. L. & Julian, B. R., 1969. Shear velocities and elastic parameters of the mantle, *J. geophys. Res.*, **74,** 6477–6501.

Anderson, D. L. & Kovach, R. L., 1969. Universal dispersion tables, III. Free oscillation variational parameters, *Bull. seism. Soc. Am.*, **59,** 1667–1693.

Anderson, D. L. & Smith, M. L., 1968. Mathematical and physical inversion of gross earth geophysical data, *Trans. Am. geophys. Un.*, **49**, 283.

Anderson, D. L. & Toksöz, M. N., 1963. Surface waves on a spherical earth, 1. Upper mantle structure from Love waves, *J. geophys. Res.*, **68**, 3483.

Archambeau, C. B., Flinn, E. A. & Lambert, D. G., 1969. Fine structure of the upper mantle, *J. geophys. Res.*, **74**, 5825–5865.

Backus, G. & Gilbert, F., 1968. The resolving power of gross earth data, *Geophys. J. R. astr. Soc.*, **16**, 169–205.

Backus, G. & Gilbert, F., 1970. Uniqueness in the inversion of inaccurate gross earth data, *Phil. Trans. R. Soc. Lond. A*, **266**, 123–192.

Birch, F., 1940. *Am. J. Sci.*, **238**, 192.

Birch, F., 1964. Density and composition of the mantle and core, *J. geophys. Res.*, **69**, 4377–4388.

Bolt, B., 1962. Gutenberg's early *PKP* observations, *Nature*, **196**, 122–124.

Bolt, B., 1968. Estimation of *PKP* travel times, *Bull. seism. Soc. Am.*, **58**, 1305–1324.

Bolt, B., Niazi, M. & Somerville, M., 1970. Diffracted *ScS* and the shear velocity at the core boundary, *Geophys. J. R. astr. Soc.*, **19**, 299–305.

Brune, J. N., 1969. Surface waves and crustal structure, *The Earth's crust and upper mantle*, Geophys. Monogr. 13, ed. P. J. Hart, Am. Geophys. Un., Wash. D.C.

Buchbinder, G. R., 1965. *PcP* from the nuclear explosion BILBY, Sept. 13, 1963, *Bull. seism. Soc. Am.*, **55**, 441–461.

Buchbinder, G. R., 1971. A velocity structure of the earth's core, *Bull. seism. Soc. Am.*, **61**, 429.

Bullen, K. E., 1946. A hypothesis on compressibility at pressures of the order of a million atmospheres, *Nature*, **157**, 405.

Bullen, K. E., 1958. Solidity of the inner core, *Contributions in honour of Beno Gutenberg*, 113–120, Pergamon Press Ltd, London.

Bullen, K. E., 1963. *Introduction to the theory of Seismology*, Cambridge University Press, 381 pp.

Bullen, K. E. & Haddon, R. A., 1967. Derivation of an earth model from free oscillation data, *Proc. Nat'l. Acad. Sci.*, **58**, 846–852.

Carder, D. S., Gordon, D. W. & Jordan, J. N., 1966. Analysis of surface-foci travel times, *Bull. seism. Soc. Am.*, **56**, 815–840.

Chinnery, M. A., 1969. Velocity anomalies in the lower mantle, *Phys. Earth Planet. Int.*, **2**. 1–10.

Cleary, J. R., 1969. The *S* velocity at the core–mantle boundary from observations of diffracted *S*, *Bull. seism. Soc. Am.*, **59**, 1399–1405.

Cleary, J. R. & Hales, A. L., 1966. An analysis of the travel times of *P* waves to North American stations in the distance range 32° to 100°, *Bull. seism. Soc. Am.*, **56**, 467–489.

Cleary, J. & Hales, A., 1970. *PKIKP* residuals at stations in North America and Europe, *Earth Planet. Sci. Lett.*, **8**, 279–282.

Corbishley, D. J., 1970. Multiple array measurements of the *P*-wave travel-time derivative, *Geophys. J. R. astr. Soc.*, **19**, 1–14.

Davies, D. & Sheppard, R. M., 1972. Lateral heterogeneity in the Earth's mantle, *Nature*, **239**, 318–323.

Derr, J. S., 1969a. Internal structure of the earth inferred from free oscillations, *J. geophys. Res.*, **74**, 5202–5220.

Derr, J. S., 1969b. Free oscillation observations through 1968, *Bull. seism. Soc. Am.*, **59**, 2079–2100.

Dorman, J., Ewing, M. & Oliver, J., 1960. Study of shear velocity distribution by mantle Rayleigh waves, *Bull. seism. Soc. Am.*, **50**, 87–175.

Doyle, H. A. & Hales, A. L., 1967. An analysis of the travel times of *S* waves to North American stations in the distance range 28° to 82°, *Bull. seism. Soc. Am.*, **57**, 761–771.

Dziewonski, A., 1971. On regional differences in dispersion of mantle Rayleigh waves, *Geophys. J. R. astr. Soc.*, **22**, 289–326.

Dziewonski, A. & Gilbert, F., 1972. Observations of normal modes from 84 recordings of the Alaskan earthquake of 1964 March 28, *Geophys. J. R. astr. Soc.*, **27**, 393–446.

Dziewonski, A. & Landisman, M., 1970. Great circle Rayleigh and Love wave dispersion from 100 to 900 *S*, *Geophys. J. R. astr. Soc.*, **19**, 37–91.

Dziewonski, A., Mills, J. & Bloch, S., 1972. Residual dispersion measurement—a new method of surface wave analysis, *Bull. seism. Soc. Am.*, **62**, 129–135.

Enayatollah, M. A., 1971. Travel times of *P*-waves for the Swedish–Finnish seismograph network, *Pure appl. Geophysics*, 101–135.

Engdahl, E. R., 1968. *Core phases and the Earth's core*, Dissertation, St Louis University.

Engdahl, E. R., 1968. Seismic waves within the earth's outer core: Multiple reflection, *Science*, **161**, 263–264.

Engdahl, E. R., Flinn, E. A. & Romney, C. F., 1970. Seismic waves reflected from the earth's inner core, *Nature*, **229**, 852–853.

Freeman, H., 1963. *Introduction to statistical inference*, Addison–Wesley, Reading.

Gilbert, F., 1971. The diagonal sum rule and average eigenfrequencies, *Geophys. J. R. astr. Soc.*, **23**, 119–123.

Gilbert, F. & Backus, G., 1968. Approximate solutions to the inverse normal mode problem, *Bull. seism. Soc. Am.*, **58**, 103–131.

Gogna, M. L., 1967. Travel times from central Pacific nuclear explosions, *Geophys. J. R. astr. Soc.*, **13**, 503–527.

Gogna, M. L., 1968. Travel time of *PKP* from Pacific earthquakes, *Geophys. J. R. astr. Soc.*, **16**, 489–514.

Green, R. W. & Hales, A. L., 1968. The travel times of *P* waves to 30° in the central United States and upper mantle structure, *Bull. seism. Soc. Am.*, **58**, 267–289.

Gutenberg, B., 1959. The asthenosphere low velocity layer, *Ann. Geofis.*, **12**, 439.

Haddon, R. A. W., 1972. Corrugations on the mantle–core boundary or transition layers between inner and outer cores? *EOS Trans. Am. geophys. Un.*, **53**, 600.

Haddon, R. A. W. & Bullen, K. E., 1969. An earth model incorporating free earth oscillation data, *Phys. Earth Planet. Int.*, **2**, 35–49.

Hai, N., 1963. Propagation des ondes longitudinales dans le noyeau terrestre, *Ann. Geophys.*, **19**, 285–346.

Hales, A., Cleary, J. & Roberts, J., 1968. Velocity distributions in the lower mantle, *Bull. seism. Soc. Am.*, **58**, 1975–1989.

Hales, A. L. & Roberts, J. L., 1970a. The travel times of *S* and *SKS*, *Bull. seism. Soc. Am.*, **60**, 461–489.

Hales, A. L. & Roberts, J. L., 1970b. Shear velocities in the lower mantle and the radius of the core, *Bull. seism. Soc. Am.*, **60**, 1427–1436.

Hales, A. L. & Roberts, J. L., 1971. The velocities in the outer core, *Bull. seism. Soc. Am.*, **61**, 1051–1059.

Helmberger, D. V. & Wiggins, R. A., 1971. Upper mantle structure of midwestern United States, *J. geophys. Res.*, **76**, 3229–3244.

Herrin, E. (chairman), 1968. 1968 Seismological Tables for *P* Phases, *Bull. seism. Soc. Am.*, **58**, 1193.

Herrin, E., Tucker, W., Taggart, J., Gordon, D. & Lobdell, J., 1968. Estimation of surface focus *P* travel times, *Bull. seism. Soc. Am.*, **58**, 1273–1291.

Ibrahim, A. K. & Nuttli, O., 1967. Travel time curves and upper mantle structure from long period *S* waves, *Bull. seism. Soc. Am.*, **57,** 1063–1092.

Jeffreys, H., 1962. Travel times for Pacific explosions, *Geophys. J. R. astr. Soc.*, **7,** 212.

Jeffreys, H., 1970. *The Earth*, 5th Ed., Cambridge University Press, Cambridge.

Jeffreys, H. & Bullen, K. E., 1940. *Seismological tables*, Brit. Assoc. Advancement of Sci., Gray–Milne Trust, London, 55 pp.

Johnson, L., 1967. Array measurements of *P* velocities in the upper mantle, *J. geophys. Res.*, **72,** 6309–6325.

Johnson, L. R., 1969. Array measurements of *P* velocities in the lower mantle, *Bull. seism. Soc. Am.*, **59,** 973–1008.

Jordan, T. H., 1972. *Estimation of the radial variation of seismic velocities and density in the earth*, Ph.D. Thesis, California Institute of Technology.

Jordan, T. H. & Anderson, D. L., 1972. Differential travel times for gross Earth studies, *EOS, Trans., A.G.U.*, **53,** 453.

Jordan, T. H. & Franklin, J., 1971. Optimal solutions to a linear inverse problem in geophysics, *Proc. Nat. Acad. Sci.*, **68,** 291–293.

Jordan, T. H. & Minster, J. B., 1972. Applications of a stochastic inverse to the geophysical inverse problem, in *The mathematics of profile inversion*, ed. L. Colin, Marcell Dekker Inc., New York.

Jordan, T. H., Minster, B. & Anderson, D. L., 1971. Resolvable features of a family of Earth models, *EOS, Trans., A.G.U.*, **52,** 287.

Julian, B. R. & Anderson, D. L., 1968. Travel times, apparent velocities and amplitudes of body waves, *Bull. seism. Soc. Am.*, **58,** 339.

Julian, B. R., Davies, D. & Sheppard, R. M., 1972. *PKJKP*, *Nature*, **235,** 317–318.

Julian, B. R. & Sengupta, M. K., 1973. Seismic travel time evidence for lateral heterogeneity in the deep mantle, *Nature*, in press.

Kanamori, H., 1967. Upper mantle structure from apparent velocities of *P* waves recorded at Wakayama micro-earthquake observatory, *Bull. Earthq. Res. Inst.*, **45,** 657–678.

Kanamori, H., 1968. Travel times to Japanese stations from LONGSHOT, *Bull. Earthq. Res. Inst.*, **46,** 811.

Kanamori, H., 1970. Velocity and *Q* of mantle waves, *Phys. Earth Planet. Int.*, **2,** 259.

Kanamori, H. & Press, F., 1970. How thick is the lithosphere?, *Nature*, **226,** 330.

Kanasewich, E. R., Ellis, R. M., Chapman, C. H. & Gutowski, P. R., 1972. Teleseismic array evidence for inhomogeneities in the lower mantle and the origin of the Hawaii Islands, *Nature Phys. Sci.*, **239,** 99–100.

Kelis-Borok, V. I. & Yanovskaya, T. B., 1967. Inverse problems of seismology, *Geophys. J. R. astr. Soc.*, **13,** 223.

Kogan, S. D., 1960. Travel times of longitudinal and transverse waves calculated from data on nuclear explosions made in the region of the Marshall Islands, *Bull. Acad. Sci. USSR* (*Izvest.*), *Geophys. Series*, 3, 246–253.

Kogan, S. D., 1968. Transit times and amplitudes of the *PcP* wave in the case of surface focus, *Izv., Earth Physics*, **3,** 3–10.

Lambert, D. G., Von Seygen, D. H., Alexander, S. S. & Galat, G. A., 1968. *LONGSHOT Experiment, Vol.* 1, Seismic Data Lab. Rpt. No. 234, Alexandria, Va.

Lewis, B. & Meyer, R. P., 1968. A seismic investigation of the upper mantle to the west of Lake Superior, *Bull. seism. Soc. Am.*, **58,** 565–596.

Lehmann, I., 1964. The Hindu Kush earthquake of March 4, 1949 as recorded in Europe, *Bull. seism. Soc. Am.*, **54,** 1915–1925.

Lomnitz, C., 1971. Travel time errors in the laterally inhomogeneous earth, *Bull. seism. Soc. Am.*, 1639–1654.

MacDonald, G. J. F. & Ness, N., 1961. A study of the free oscillations of the earth, *J. geophys. Res.*, **66**, 1865–1911.
Mueller, G., 1973. Amplitude studies of core phases, *J. geophys. Res.*, in press.
Muirhead, K. J. & Cleary, J. R., 1969. Comparison of the 1968 *P* tables with times fron nuclear explosions (II), The Marshall Islands and Sahara series, *Earth Planet. Sci. Lett.*, **7**, 132–136.
Niazi, M. & Anderson, D. L., 1965. Upper mantle structure of western North America from apparent velocities of *P* waves, *J. geophys. Res.*, **70**, 4633–4640.
Nuttli, O. W., 1969. Travel times and amplitudes of *S* waves from nuclear explosions in Nevada, *Bull. seism. Soc. Am.*, **59**, 385–398.
Pekeris, C. L., 1966. The internal constitution of the Earth, *Geophys. J. R. astr. Soc.*, **11**, 85–132.
Press, F., 1968. Earth models obtained by Monte Carlo inversion, *J. geophys. Res.*, **73**, 5223–5234.
Press, F., 1970. Earth models consistent with geophysical data, *Phys. Earth Planet. Int.*, **3**, 3–22.
Press, F., 1972. The earth's interior as inferred from a family of models, in *The nature of the solid Earth*, ed. E. Robertson, McGraw–Hill, Inc.
Randall, M. J., 1971. A revised travel-time table for *S*, *Geophys. J. R. astr. Soc.*, **22**, 229–234.
Richards, P., 1973. Calculations of body waves, for caustics and tunnelling in core phases, *Geophys. J. R. astr. Soc.*, **35**, 243.
Shadidi, M., 1968. Variation of amplitude of *PKP* across the caustic, *Phys. Earth Planet. Int.*, **1**, 97–102.
Sutton, G. H. & Walker, D. A., 1972. Oceanic mantle phases recorded on seismographs in the northwestern Pacific at distances between 7° and 40°, *Bull. seism. Soc. Am.*, **62**, 631–656.
Taggert, J. N. & Engdahl, E. R., 1968. Estimation of *PcP* travel times and the depth to the core, *Bull. seism. Soc. Am.*, **58**, 1293–1303.
Toksöz, M. N. & Ben-Menahem, A., 1963. Velocities of mantle Love and Rayleigh waves over multiple paths, *Bull. seism. Soc. Am.*, **53**, 741–764.
Wang, C., 1972. A simple earth model, *J. geophys. Res.*, **77**, 4318–4329.
Whitcomb, J. H., 1973. Part I. *A study of the velocity structure of the earth by the use of core phases*, Ph.D. Thesis, California Institute of Technology,
Whitcomb, J. H. & Anderson, D. L., 1970. Reflection of *P'P'* (*PKPPKP*) seismic waves from discontinuities in the mantle, *J. geophys. Res.*, **75**, 5713–5728.
Wiggins, R. A., 1968. Terrestrial variation tables for the periods and attenuation of the free oscillations, *Phys. Earth Planet. Int.*, **1**, 201.

Table A1

Observed and theoretical periods of spheroidal oscillations. Data for ${}_0S_2$ *and* ${}_0S_3$ *from Derr* (1969b, *Table* 5)*; data for* ${}_0S_{51}-{}_0S_{63}$ *from Dziewonski* (1971), *Table* 2)*; all other data from Dziewonski & Gilbert* (1972, *Tables* 2 *and* 4)

Mode	Observed data				Model BI	
	Period (s)	S.E.M. (s)	95% C.I. (s)	95% C.I. %	Period (s)	Rel. error %
${}_0S_0$	1227·65	0·68	1·44	0·12	1227·61	0·00
${}_1S_0$	613·57	0·24	0·54	0·09	614·09	0·08
${}_2S_0$	398·54	0·08	0·16	0·04	398·49	−0·01

Table A1 (*continued*)

Mode	Observed data Period (s)	S.E.M. (s)	95% C.I. (s)	95% C.I. %	Model B1 Period (s)	Rel. error %
${}_3S_0$	305·84	0·13	0·32	0·11	305·53	−0·10
${}_4S_0$	243·59	0·07	0·15	0·06	243·55	−0·02
${}_0S_2$	3233·30	0·50	0·98	0·03	3232·45	−0·03
${}_0S_3$	2133·56	0·38	0·86	0·04	2134·13	0·03
${}_0S_4$	1547·30	0·88	1·76	0·11	1545·82	−0·10
${}_0S_5$	1190·12	0·43	0·86	0·07	1190·42	0·03
${}_0S_6$	963·17	0·29	0·58	0·06	963·72	0·06
${}_0S_7$	811·45	0·25	0·50	0·06	812·24	0·10
${}_0S_8$	707·64	0·14	0·28	0·04	707·70	0·01
${}_0S_9$	633·95	0·10	0·20	0·03	633·69	−0·04
${}_0S_{10}$	580·08	0·10	0·18	0·03	579·19	−0·15
${}_0S_{11}$	536·56	0·11	0·22	0·04	536·87	0·06
${}_0S_{12}$	502·18	0·07	0·14	0·03	502·34	0·03
${}_0S_{13}$	473·14	0·07	0·14	0·03	473·21	0·02
${}_0S_{14}$	448·28	0·05	0·10	0·02	448·10	−0·04
${}_0S_{15}$	426·24	0·05	0·10	0·02	426·16	−0·02
${}_0S_{16}$	406·77	0·05	0·10	0·03	406·79	0·01
${}_0S_{17}$	389·31	0·07	0·14	0·04	389·56	0·06
${}_0S_{18}$	373·89	0·07	0·14	0·04	374·10	0·06
${}_0S_{19}$	360·20	0·06	0·12	0·03	360·14	−0·02
${}_0S_{20}$	347·82	0·07	0·14	0·04	347·47	−0·10
${}_0S_{21}$	336·00	0·06	0·12	0·04	335·88	−0·04
${}_0S_{22}$	325·31	0·06	0·12	0·04	325·23	−0·02
${}_0S_{23}$	315·43	0·04	0·08	0·03	315·38	−0·02
${}_0S_{24}$	306·25	0·05	0·10	0·03	306·24	−0·00
${}_0S_{25}$	297·71	0·05	0·10	0·04	297·72	0·00
${}_0S_{26}$	289·69	0·05	0·10	0·04	289·74	0·02
${}_0S_{27}$	282·34	0·07	0·14	0·05	282·25	−0·03
${}_0S_{28}$	275·06	0·05	0·10	0·04	275·18	0·04
${}_0S_{29}$	268·44	0·05	0·10	0·04	268·49	0·02
${}_0S_{30}$	262·15	0·05	0·10	0·04	262·15	0·00
${}_0S_{31}$	256·00	0·06	0·12	0·05	256·12	0·05
${}_0S_{32}$	250·20	0·06	0·12	0·05	250·38	0·07
${}_0S_{33}$	244·95	0·06	0·12	0·05	244·91	−0·02
${}_0S_{34}$	239·70	0·07	0·14	0·06	239·67	−0·01
${}_0S_{35}$	234·69	0·07	0·14	0·06	234·66	−0·01
${}_0S_{36}$	229·74	0·07	0·14	0·06	229·85	0·05
${}_0S_{37}$	225·16	0·05	0·10	0·04	225·24	0·03
${}_0S_{38}$	220·62	0·05	0·10	0·05	220·80	0·08
${}_0S_{39}$	216·43	0·05	0·10	0·05	216·54	0·05
${}_0S_{40}$	212·31	0·09	0·18	0·09	212·43	0·06
${}_0S_{41}$	208·05	0·12	0·25	0·12	208·47	0·20
${}_0S_{42}$	204·57	0·07	0·14	0·07	204·65	0·04
${}_0S_{43}$	200·93	0·08	0·16	0·08	200·96	0·02
${}_0S_{44}$	197·19	0·08	0·16	0·08	197·40	0·11
${}_0S_{45}$	194·03	0·07	0·14	0·07	193·95	−0·04
${}_0S_{46}$	190·59	0·09	0·18	0·09	190·62	0·02
${}_0S_{47}$	187·43	0·05	0·11	0·06	187·40	−0·02
${}_0S_{48}$	184·25	0·09	0·19	0·10	184·27	0·02
${}_0S_{49}$	181·30	0·11	0·23	0·13	181·24	−0·03
${}_0S_{50}$	178·35	0·12	0·25	0·14	178·83	−0·02
${}_0S_{51}$	175·42	0·03	0·06	0·03	175·46	0·02
${}_0S_{52}$	172·64	0·03	0·06	0·04	172·70	0·03
${}_0S_{53}$	169·97	0·03	0·06	0·04	170·01	0·03
${}_0S_{54}$	167·38	0·03	0·06	0·04	167·41	0·02
${}_0S_{55}$	164·85	0·03	0·06	0·04	164·87	0·02
${}_0S_{56}$	162·41	0·03	0·06	0·04	162·41	0·00
${}_0S_{57}$	160·01	0·03	0·06	0·04	160·02	0·00
${}_0S_{58}$	157·70	0·04	0·08	0·05	157·69	−0·01
${}_0S_{59}$	155·45	0·04	0·08	0·05	155·42	−0·02

Table A1 (*continued*)

Mode	Observed data Period (s)	S.E.M. (s)	95% C.I. (s)	%	Model B1 Period (s)	Rel. error %
${}_0S_{60}$	153·24	0·04	0·08	0·05	153·21	−0·02
${}_0S_{61}$	151·12	0·04	0·08	0·05	151·06	−0·04
${}_0S_{62}$	149·07	0·04	0·08	0·05	148·96	−0·07
${}_0S_{63}$	147·09	0·05	0·11	0·08	146·92	−0·12
${}_1S_2$	1470·85	1·28	2·60	0·18	1469·05	−0·12
${}_1S_3$	1060·83	0·99	2·05	0·19	1062·76	0·10
${}_1S_4$	852·68	0·37	0·74	0·09	851·75	−0·11
${}_1S_5$	730·56	0·44	1·00	0·14	729·30	−0·17
${}_1S_6$	657·61	0·20	0·41	0·06	656·94	−0·10
${}_1S_7$	603·93	0·31	0·63	0·10	604·25	0·05
${}_1S_8$	555·83	0·16	0·16	0·03	556·22	0·07
${}_1S_9$	509·58	0·20	0·43	0·08	509·86	0·06
${}_1S_{10}$	465·45	0·29	0·63	0·14	466·20	0·16
${}_1S_{14}$	337·00	0·08	0·16	0·05	336·64	−0·11
${}_1S_{15}$	316·06	0·08	0·17	0·05	315·59	−0·15
${}_1S_{16}$	299·87	0·15	0·33	0·11	299·47	−0·14
${}_1S_{17}$	285·97	0·13	0·29	0·10	286·10	0·04
${}_2S_1$	1058·09	0·89	2·06	0·20	1057·92	−0·02
${}_2S_2$	904·23	0·49	1·04	0·12	904·50	0·03
${}_2S_3$	804·17	0·51	1·10	0·14	805·04	0·11
${}_2S_4$	724·87	0·23	0·45	0·06	725·02	0·02
${}_2S_6$	594·71	0·14	0·29	0·05	594·60	−0·02
${}_2S_8$	488·02	0·15	0·33	0·07	487·65	−0·08
${}_2S_9$	448·36	0·13	0·29	0·07	448·37	0·00
${}_2S_{10}$	415·67	0·16	0·33	0·08	415·89	0·05
${}_2S_{11}$	388·27	0·23	0·55	0·14	388·54	0·07
${}_2S_{12}$	365·12	0·19	0·40	0·11	365·13	0·00
${}_2S_{13}$	344·88	0·19	0·44	0·13	344·71	−0·05
${}_2S_{14}$	326·26	0·12	0·25	0·08	326·44	0·06
${}_2S_{15}$	309·20	0·06	0·15	0·05	308·95	−0·08
${}_3S_2$	580·80	0·70	1·40	0·24	580·49	−0·05
${}_3S_3$	489·05	0·36	0·82	0·17	488·00	−0·22
${}_3S_4$	439·18	0·48	1·05	0·24	438·79	−0·09
${}_3S_5$	415·11	0·22	0·51	0·12	414·87	−0·06
${}_3S_6$	392·32	0·11	0·22	0·08	392·42	0·03
${}_3S_7$	372·05	0·13	0·28	0·08	372·45	0·11
${}_3S_8$	354·57	0·11	0·23	0·07	354·86	0·08
${}_3S_9$	339·14	0·15	0·32	0·09	339·02	−0·03
${}_3S_{10}$	323·80	0·11	0·23	0·07	324·41	0·19
${}_3S_{11}$	310·77	0·08	0·20	0·06	310·68	−0·03
${}_4S_1$	505·82	0·21	0·45	0·09	504·14	−0·33
${}_4S_2$	479·33	0·19	0·38	0·08	478·00	−0·28
${}_4S_3$	460·78	0·15	0·30	0·07	460·93	0·03
${}_4S_4$	420·10	0·09	0·19	0·05	420·22	0·03
${}_4S_5$	369·72	0·07	0·15	0·04	369·88	0·04
${}_4S_6$	332·11	0·08	0·18	0·05	332·15	0·01
${}_4S_7$	303·97	0·09	0·19	0·06	303·95	−0·01
${}_4S_8$	283·56	0·10	0·21	0·07	283·83	0·10
${}_4S_9$	269·66	0·06	0·13	0·05	269·90	0·09
${}_4S_{10}$	258·86	0·05	0·10	0·04	259·03	0·06
${}_5S_2$	397·36	0·16	0·36	0·09	396·78	−0·15
${}_5S_3$	353·52	0·17	0·42	0·12	354·22	0·20
${}_6S_1$	348·41	0·05	0·10	0·03	348·32	−0·03
${}_6S_4$	293·19	0·13	0·25	0·10	293·13	−0·02
${}_6S_5$	273·52	0·05	0·11	0·04	273·25	−0·02
${}_7S_2$	310·07	0·08	0·17	0·06	309·58	−0·16
${}_7S_3$	282·37	0·11	0·25	0·09	281·22	−0·05
${}_7S_5$	239·96	0·03	0·06	0·03	239·90	−0·03
${}_8S_1$	272·10	0·14	0·31	0·11	271·44	−0·24
${}_8S_2$	247·74	0·02	0·05	0·02	248·71	0·39

Table A2

Observed and theoretical periods of toroidal oscillations. Datum for ${}_0T_2$ from Derr (1969b, Table 5); all other data from Dziewonski & Gilbert (1972, Tables 3 and 5)

	Observed data				Model B1	
Mode	Period (s)	S.E.M. (s)	95% C.I. (s)	95% C.I. %	Period (s)	Rel. error %
${}_0T_2$	2640·63	10·10	23·84	0·90	2630·81	−0·37
${}_0T_3$	1705·83	2·53	5·47	0·32	1702·43	−0·21
${}_0T_4$	1305·45	0·93	1·91	0·15	1303·53	−0·15
${}_0T_5$	1075·97	0·82	1·68	0·16	1075·30	−0·06
${}_0T_6$	925·83	0·53	1·11	0·12	925·26	−0·06
${}_0T_7$	819·31	0·68	1·41	0·17	817·76	−0·19
${}_0T_8$	736·86	0·34	0·68	0·09	736·13	−0·10
${}_0T_9$	671·80	0·37	0·74	0·11	671·53	−0·04
${}_0T_{10}$	618·98	0·29	0·58	0·09	618·84	−0·02
${}_0T_{11}$	574·62	0·47	0·96	0·17	574·82	0·04
${}_0T_{12}$	536·84	0·34	0·70	0·13	537·37	0·10
${}_0T_{13}$	504·94	0·41	0·84	0·17	505·02	0·02
${}_0T_{14}$	475·73	0·36	0·75	0·16	476·73	0·21
${}_0T_{15}$	450·97	0·26	0·54	0·12	451·71	0·16
${}_0T_{16}$	429·19	0·27	0·56	0·13	429·40	0·05
${}_0T_{17}$	407·95	0·20	0·42	0·10	409·35	0·34
${}_0T_{18}$	390·94	0·28	0·58	0·15	391·20	0·07
${}_0T_{19}$	374·75	0·17	0·36	0·10	374·68	−0·02
${}_0T_{20}$	359·59	0·29	0·62	0·17	359·57	−0·01
${}_0T_{21}$	345·82	0·30	0·65	0·19	345·67	−0·04
${}_0T_{22}$	332·57	0·22	0·49	0·15	332·85	0·09
${}_0T_{23}$	321·21	0·29	0·63	0·20	320·98	−0·07
${}_0T_{24}$	310·18	0·25	0·55	0·18	309·95	−0·08
${}_0T_{25}$	299·51	0·21	0·51	0·17	299·66	0·05
${}_0T_{26}$	290·26	0·16	0·39	0·13	290·05	−0·07
${}_0T_{27}$	281·21	0·44	1·13	0·40	281·05	−0·06
${}_0T_{28}$	272·75	0·27	0·61	0·22	272·59	−0·06
${}_0T_{29}$	264·53	0·32	1·01	0·39	264·64	0·04
${}_0T_{30}$	257·29	0·38	1·01	0·39	257·14	−0·06
${}_0T_{31}$	249·85	0·24	0·59	0·24	250·05	0·08
${}_0T_{32}$	242·97	0·25	0·59	0·24	243·35	0·16
${}_0T_{33}$	236·71	0·24	0·62	0·26	237·00	0·12
${}_0T_{34}$	231·29	0·23	0·64	0·28	230·97	−0·14
${}_0T_{35}$	224·93	0·35	0·86	0·38	225·24	0·14
${}_0T_{36}$	219·69	0·25	0·64	0·29	219·79	0·04
${}_0T_{37}$	213·89	0·21	0·67	0·31	214·59	0·33
${}_0T_{38}$	209·83	0·59	2·54	1·21	209·65	−0·09
${}_0T_{39}$	204·27	0·01	0·43	0·21	204·92	0·32
${}_0T_{40}$	199·96	0·38	1·06	0·53	200·39	0·22
${}_0T_{41}$	195·88	0·43	1·20	0·61	196·05	0·09
${}_0T_{42}$	191·26	0·25	0·70	0·37	191·91	0·34
${}_0T_{43}$	187·40	0·49	0·21	0·11	187·93	0·28
${}_0T_{44}$	183·78	0·27	0·75	0·41	184·12	0·18
${}_0T_{45}$	180·25	0·06	0·19	0·11	180·45	0·11
${}_0T_{46}$	176·85	0·06	0·19	0·11	176·93	0·05
${}_1T_2$	756·57	0·63	1·36	0·18	756·80	0·03
${}_1T_3$	695·18	0·52	1·10	0·16	694·41	−0·11
${}_1T_4$	629·98	0·63	1·74	0·28	630·50	0·08
${}_1T_6$	519·09	0·30	0·68	0·13	519·46	0·07
${}_1T_8$	438·50	0·23	0·59	0·14	438·89	0·09
${}_1T_{10}$	381·58	0·15	0·33	0·09	382·07	0·13
${}_2T_4$	421·81	0·36	0·78	0·19	420·62	−0·28
${}_2T_7$	363·66	0·28	0·62	0·17	363·47	−0·05
${}_2T_8$	343·46	0·22	0·50	0·15	343·48	0·00

Table A3

Observed and theoretical differential travel times (surface and deep (600 km) focus) PcP–P, $P'_{AB}-P'_{DF}$, $P'_{BC}-P'_{DF}$, *and* ScS–S. *Data are the raw cell means given by Jordan* (1972, *Table A*3·5)

(deg)	Obs. time (s)	S.E.M. (s)	95% C.I. (s)	B1 time (s)	Residual (s)
			PcP–P (surface focus)		
30·00	181·9	0·18	0·39	181·0	−0·9
35·00	151·4	0·14	0·30	151·3	−0·1
40·00	125·1	0·22	0·46	124·5	−0·6
45·00	100·7	0·22	0·43	100·8	+0·1
50·00	79·9	0·19	0·39	79·9	0·0
55·00	62·3	0·45	1·02	61·8	−0·5
60·00	46·1	0·45	0·99	46·1	0·0
65·00	33·0	0·43	0·95	32·8	−0·2
70·00	22·1	1·11	2·72	21·8	−0·3
75·00	13·4	0·76	2·12	13·3	−0·1
			PcP–P (deep focus)		
30·00	162·2	0·27	0·69	161·7	−0·5
35·00	133·1	0·78	2·17	134·1	+1·0
40·00	109·1	0·81	2·58	109·4	+0·3
45·00	87·3	0·28	0·61	87·8	+0·5
50·00	68·8	0·06	0·13	68·8	0·0
55·00	52·5	0·19	0·53	52·4	−0·1
60·00	37·5	0·23	0·49	38·3	+0·8
65·00	25·9	0·27	0·59	26·5	+0·6
70·00	17·2	0·25	0·59	17·0	−0·2
			$P'_{AB}-P'_{DF}$ (deep focus)		
147·50	7·7	0·24	0·51	7·8	+0·1
152·50	20·6	0·28	0·58	20·9	+0·3
157·50	35·1	0·19	0·39	35·7	+0·6
165·00	60·8	0·31	0·64	60·7	−0·1
			$P'_{BC}-P'_{DF}$ (deep focus)		
146·25	2·5	0·30	0·71	2·5	0·0
148·75	4·9	0·11	0·23	5·3	+0·4
151·25	7·6	0·20	0·42	7·9	+0·3
153·75	9·0	0·24	0·58	10·3	+1·3
156·25	10·8	0·34	0·77	12·6	+1·8
			ScS–S (deep focus)		
30·00	311·3	0·80	1·77	308·3	−3·0
35·00	259·4	0·71	1·53	259·0	−0·4
40·00	215·7	0·66	1·62	214·6	−1·1
45·00	174·3	0·52	1·11	175·0	+0·7
50·00	138·6	0·69	1·44	139·4	+0·8
55·00	108·5	0·58	1·25	108·7	+0·2
60·00	82·0	0·52	1·07	82·2	+0·2
65·00	59·7	0·44	0·92	59·4	−0·3
70·00	40·6	0·46	0·96	40·6	−0·0
75·00	25·5	0·60	1·25	25·6	+0·1
80·00	14·0	0·37	0·80	14·4	+0·4

Table A4

Observed and theoretical differential travel times (surface focus) for the phase combinations SKKS−SKS *and* SKS−S. *Data from Hales & Roberts* (1971, *equation* 3, 1970*a*, *Table* 4)

	SKKS−SKS		*SKS−S*	
Δ (deg)	Obs (s)	B1 (s)	Obs (s)	B1 (s)
85	8·2	6·4	6·4	7·0
90	15·4	13·4	22·0	24·9
95	23·9	22·8	39·4	42·6
100	33·9	33·9	—	—
105	45·2	46·2	—	—
110	57·9	59·4	—	—
115	72·0	73·5	—	—
120	87·6	88·5	—	—
125	104·8	104·5	—	—

Table A5

Travel times and dT/dΔ*'s (surface focus) for* P*-waves between* 30° *and* 95°

	t (s)			*dt*/*d*Δ (sec/deg)			
Δ (deg)	J–B (1)	'68 (2)	B1	H.C.R. (3)	C. (4)	L.J. (5)	B1
30	372·5	369·5	370·9	8·94	9·13	8·92	8·85
35	416·1	413·3	414·3	8·60	8·70	8·60	8·57
40	458·1	455·7	456·5	8·26	8·26	8·38	8·26
45	498·9	496·4	497·0	7·91	8·11	7·90	7·92
50	538·0	535·2	535·6	7·56	7·52	7·51	7·56
55	575·4	572·2	572·6	7·21	7·19	7·22	7·24
60	610·7	607·4	608·0	6·86	6·95	6·75	6·91
65	644·0	640·9	641·7	6·50	6·69	6·53	6·59
70	675·4	672·7	673·6	6·14	6·21	6·24	6·19
75	705·0	702·6	703·5	5·77	5·88	5·83	5·78
80	732·7	730·6	731·5	5·40	5·47	5·48	5·38
85	758·5	756·6	757·4	5·03	4·95	4·93	4·99
90	782·7	780·7	781·5	4·66	4·60	4·65	4·72
95	805·7	803·9	804·6	4·28	4·52	4·48	4·55

(1) Jeffreys & Bullen (1940)

(2) Herrin *et al.* (1968)

(3) Hales *et al.* (1968)

(4) Corbishley (1970)

(5) Johnson (1969)

Table A6

Travel times and dT/dΔ*'s (surface focus) for* S*-waves between* 30° *and* 95°

Δ (deg)	*t* (s) J–B (1)	H.R. (2)	B1	*dt*/*d*Δ (s/deg) H.R. (2)	B1
30	670·2	669·5	675·0	15·4	15·7
35	748·2	749·0	752·8	15·3	15·4
40	824·5	825·7	828·8	15·2	15·0
45	897·9	899·5	902·5	14·5	14·5
50	968·6	970·5	973·9	13·9	14·1
55	1036·8	1038·7	1043·2	13·4	13·5
60	1102·6	1104·1	1109·2	12·8	12·9
65	1165·5	1166·7	1172·5	12·2	12·4
70	1225·6	1226·4	1233·2	11·7	11·8
75	1282·6	1283·2	1290·6	11·1	11·2
80	1336·5	1337·3	1344·8	10·5	10·5
85	1387·3	1388·5	1395·7	10·0	9·9
90	1435·5	1436·9	1443·7	9·4	9·3
95	1478·2	1482·4	1488·6	8·8	8·7

(1) Jeffreys & Bullen (1940)

(2) Hales & Roberts (1970a)

Table A7

Travel times (surface focus) of PcP *and* ScS *at distances greater than* 30°

Δ (deg)	*PcP* J–B (s)	'68 (s)	B1 (s)	*ScS* J–B (s)	B1 (s)
30	554·9	552·1	551·9	1011·0	1016·4
35	568·6	565·9	565·7	1036·4	1042·0
40	583·9	581·1	581·0	1064·6	1070·5
45	600·5	697·7	597·7	1095·1	1101·5
50	618·3	615·5	615·6	1127·8	1134·8
55	637·0	634·3	634·4	1162·5	1169·9
60	656·6	653·9	654·1	1198·8	1206·6
65	676·9	674·2	674·5	1236·4	1244·7
70	697·8	695·1	695·5	1275·2	1283·9
75	719·1	716·5	716·9	1315·0	1323·9
80	740·6	738·0	738·5	1355·5	1364·6
85	762·3	759·9	760·5	1396·5	1405·8
90	784·2	781·9	782·7	1437·8	1447·3
95	—	—	—	1479·2	1489·0

Tables A8

Travel times (surface focus) of PKP

Δ (deg)	J–B (1) (s)	'68 (2) (s)	B1 (s)
A			
170	1286·3	1283·7	1283·4
160	1242·7	1239·7	1239·3
150	1200·2	1196·9	1196·8
145 B	1180·4	1178·0	1177·4
145 B	1179·3	1174·4	1177·4
150	—	1188·1	1191·8
155	—	1201·0	1204·3
C			
110 D	1113·2	1113·0	1114·0
120	1132·7	1132·1	1132·7
130	1152·0	1151·3	1151·4
140	1170·5	1170·1	1169·5
150	1187·4	1186·8	1186·2
160	1200·8	1200·0	1200·0
170	1209·2	1208·4	1208·9
180 F	1212·2	1211·0	1212·1

(1) Jeffreys & Bullen (1940)

(2) Bolt (1968)

Table A9

Travel times (surface focus) of PKiKP

Δ (deg)	E.F.R. (1) (s)	B1 (s)
10	996·9	996·2
20	1000·1	999·6
30	1005·7	1005·1
40	1013·2	1012·7
50	1022·8	1022·3

(1) Engdahl *et al.* (1970, Table 1).